

**Automated segmentation and reconstruction of structural elements
for indoor multi-level room environment**

Amr Nabil Amer

A Thesis

In the Department of

Building, Civil, and Environmental Engineering

Presented in Partial Fulfillment of the Requirements

For the Degree of

Master of Applied Sciences (Civil Engineering) at

Concordia University

Montreal, Quebec, Canada

March 2020

© Amr Amer, 2020

CONCORDIA UNIVERSITY
School of Graduate Studies

This is to certify that the thesis prepared

By: Amr Nabil Amer

Entitled: An automatic 3D reconstruction approach for multi-level building spaces using 3D point cloud data

and submitted in partial fulfillment of the requirements for the degree of

Master of Applied Science in Civil Engineering

complies with the regulations of the University and meets the accepted standards with respect to originality and quality.

Signed by the final Examining Committee:

_____ Chair
Dr. Osama Moselhi

_____ Examiner
Dr. Arash Mohammadi

_____ Examiner
Dr. Joonhee Lee

_____ Thesis Supervisor (s)
Dr. Sang Hyeok Han

Dr. Zhenhua Zhu

Approved by _____

Dr. Michelle Nokken, Graduate Program Director

23rd March 2020

Dr. Amir Asif, Dean, Gina Cody School of Engineering and Computer Science

ABSTRACT

An automatic 3D reconstruction approach for multi-level building spaces using 3D point cloud data

Amr Nabil Amer

3D laser scanners provide accurate as-built conditions for the surrounding environment in the form of 3D point cloud data. Although this technology has had high attention from the construction industry for the as-built documentation of buildings, the reconstruction process, especially identification and segmentation of the building elements, still has manual and labor-intensive tasks leading to time-consuming and human errors. In addition, it has not reconstructed the building elements successfully yet in multi-level building spaces. In an effort to address these issues, this research proposes an automatic 3D reconstruction framework that identifies, segments, and reconstructs vertical and horizontal building elements from the point clouds of multi-level building spaces. The proposed framework composes of: (1) identifying locations, diameters, lengths and the number of vertical building elements using Hough line and circle transform; (2) comparing the dimensions of the walls to determine single- or multi-level building spaces; (3) developing the region of interest defined by the building codes; (4) implementing plane RANSAC for not only segmentation of the vertical building elements but also identification and segmentation of horizontal building elements; and (5) reconstructing the segmented building elements into simple forms. The effectiveness of the proposed methodology has been validated with high accuracy and low deviation in three different building spaces at Concordia University, Montreal, Canada.

ACKNOWLEDGMENTS

Words cannot express my love, appreciation, respect, and gratefulness I feel towards my family, supervisors, and friends.

First and foremost, I want to thank God for everything I was, am and will be. I would like to express my very great appreciation and love to my amazing family (especially Lola), and friends for their endless support and standing by my side during this long/rough journey. This could not have been achieved without them (I LOVE YOU ALL).

I would also wish to express my deepest gratitude to Dr. Zhenhua Zhu and Dr. Sang Hyeok Han my instructors and supervisors for their patient guidance, endless support, great advice, encouragement, and wisdom. I would not be here without their supervision.

My grateful thanks are also extended to my examiners, I am gratefully indebted to Dr. Osama Moselhi, Dr. Joonhee Lee, and Dr. Arash Mohammadi not only for their valuable time and effort in reviewing my thesis but also their constructive advice to improve it.

I would like to acknowledge my indebtedness and render my warmest thanks to all colleagues in the lab office especially, Xiaoning Ren, Wenjing Chu, Yusheng Huang, and Chen Chen. Thank you all for your support. It was my pleasure to work and have this amazing experience with them.

TABLE OF CONTENTS

TABLE OF CONTENTS.....	v
LIST OF FIGURES	viii
LIST OF TABLES	ix
LIST OF ACRONYMS	xi
CHAPTER 1: INTRODUCTION.....	1
1.1 Background and Motivation.....	1
1.2 Problem Statement	5
1.3 Research Hypothesis	6
1.4 Objectives and Scopes.....	6
1.5 Expected Contributions	7
1.6 Thesis Organization.....	8
CHAPTER 2: LITERATURE REVIEW.....	9
2.1 Identification & Segmentation of Building Elements	9
2.1.1 General Methods.....	10
2.1.2 Feature-Based Methods.....	11
2.1.3 Geometry-Based Methods.....	13
2.2 Surface Reconstruction.....	15
2.3 Research gaps and objectives.....	16
CHAPTER 3: METHODOLOGY	17

3.1 Pre-processing.....	19
3.2 Transforming 3D point cloud to 2D image	21
3.3 Identification and segmentation.....	23
3.3.1 Vertical Plane Building Elements	24
3.3.2 Horizontal Plane Building Elements	28
3.4 Surface Reconstruction.....	32
3.5 Evaluation Matrix.....	33
CHAPTER 4: IMPLEMENTATION AND RESULTS	36
4.1 Implementation.....	36
4.1.1 Environments.....	36
4.1.2 Hardware.....	39
4.1.3 Software	41
4.2 Results.....	43
4.2.1 Vertical plane building elements.....	43
4.2.2 Horizontal plane building elements.....	45
4.2.3 Evaluation	47
CHAPTER 5: CONCLUSION AND FUTURE WORKS.....	51
5.1 Summary	52
5.2 Future Works	53
BIBLIOGRAPHY	54

APPENDIX..... 61

LIST OF FIGURES

Figure 1- 1: (a) Notre-Dame de Paris, (b) Tragic accident of the Notre-Dame burning down, (c) Notre-Dame 3D model in Assassins Creed game, and (d) Notre-Dame 3D-PCD (Eric Levenson, 2019; Gilbert, 2019; Tallon, 2014; Ubisoft, 2019).....	3
Figure 1- 2: Concordia University EV building Entrance Hall 3D-PCD.....	4
Figure 2- 1: Slicing the bridge’s 3D-PCD in the X direction (R. Lu et al., 2019).....	10
Figure 2- 2: (a) Point Cloud, (b) Feature detection, (c) Region growing, and (d) Final segmentation (Dimitrov & Golparvar-Fard, 2015).....	12
Figure 2- 3: (a) Slice from the 3D-PCD at ceiling level, (b) generating the image, and (c) Region growing output (Macher et al., 2015).....	12
Figure 2- 4: RANSAC family (Choi et al., 1997).....	14
Figure 3- 1: An overview of the proposed methodology	18
Figure 3- 2: 3D-point cloud data	20
Figure 3- 3: (a) 3D point cloud, (b) Projecting the 3D point cloud on a 2D plane, (c) Canny edge detection, and (d) Threshold and Binary	23
Figure 3- 4: Identification and segmentation of a column	25
Figure 3- 5: Identification and segmentation of walls.....	27
Figure 3- 6: (a) Horizontal plane elements region of interests and (b) Pseudocode of process flow	31
Figure 3- 7: Surface reconstruction procedure.....	33
Figure 4- 1: (a) EV building, and (b) EV building location in SGW Campus (Concordia University, 2019).....	37
Figure 4- 2: (a) Lab office 3D-PCD, and (b) Lab office 2D plane and scan locations.....	38

Figure 4- 3: (a) EV entrance hall 3D-PCD, and (b) EV entrance hall 2D plane and scan locations	38
Figure 4- 4: (a) Auditorium 3D-PCD, and (b) Auditorium 2D plane and scan locations.....	38
Figure 4- 5: Laser scanner and spherical reference targets deployment	40
Figure 4- 6: Registering the 3D-PCD using Trimble Real Works software.....	42
Figure 4- 7: Cleaning the 3D- PCD from outliers using CloudCompare software	43
Figure 4- 8: Applying colors to the final 3D reconstructed model using Blender software	43
Figure 4- 9: Identification and segmentation of columns	44
Figure 4- 10: Identification and segmentation of ceilings	46
Figure 4- 11: Floors and stairs identification and segmentation.....	47
Figure 4- 12: Reconstruction results of Lab office, EV entrance hall, and auditorium (sidewall #4 is removed for visualization in both the lab and auditorium case studies).....	49
Figure 6- 1: Results of each step in the Proposed methodology for the lab office case study	63
Figure 6- 2: Flowchart for the case of lab office case study	64
Figure 6- 3: Results of each step in the Proposed methodology for the EV entrance hall case study	65
Figure 6- 4: Flowchart for the case of EV entrance hall case study	66
Figure 6- 5: Results of each step in the Proposed methodology for auditorium case study	67
Figure 6- 6: Flowchart for the case of auditorium case study	68

LIST OF TABLES

Table 1- 1: Titles and summary of each chapter of this Thesis.....	8
Table 3- 1: Parameters of each building element.....	35
Table 4- 1: Case study information.....	39
Table 4- 2: Technical specifications for the laser scanner (Faro Inc., 2020; Lafi, 2017)	41
Table 4- 3: Technical specifications for the Laptop (Inc., 2020; Lafi, 2017).....	41
Table 4- 4: Results of the evaluation matrix.....	49
Table 4- 5: Results of the size difference and deviation.....	51
Table 6- 1: Software results in the reconstruction process.....	62
Table 6- 2: Building elements characteristics.....	69
Table 6- 3: Building Code of Ontario (ONTARIO, 2017).....	69

LIST OF ACRONYMS

RANSAC	Random sample consensus
CHT	Circle Hough transform
LHT	Line Hough transform
3D-PCD	Three-dimensional point cloud data
I&S	Identification and segmentation
RGB	Red-Green-Blue
STL	Standard Triangle Language (stereolithography)
DWG	AutoCAD Drawing Database
HPE	Horizontal Plane Elements
VBE	Vertical Building Elements
TOF	Time of Flight
FOV	Field of View
MLESAC	Maximum Likelihood Estimation Sample and Consensus
EV Building	Engineering, Computer Science and Visual Arts Integrated Complex
BIM	Building Information Modeling
2D	Two dimensional

USD	United States dollar
LIDAR	Laser identification detection and ranging
BE	Building elements
HT	Hough Transform
AEC	Architecture, engineering, and construction
HVAC	Heating, Ventilation, and Air Conditioning
Voxel	Volume Pixel

CHAPTER 1: INTRODUCTION

This research aims to propose a framework to automatically identify, segment and reconstruct building elements such as columns, walls, ceilings, floors, and stairs from 3D point cloud data (3D-PCD) using multiple algorithms such as Hough transform and RANSAC. The upcoming sections in this chapter describe the research background, motivation, objectives, contribution, and the organization of the thesis.

1.1 Background and Motivation

According to the investigation reported by Canadian home builders' association in 2017, the building renovation and remodeling projects in Canada are total \$ 77.9 billion and \$ 41.3 billion USD in wages (association, 2019). A significant amount of these wages is attributed to reworks (e.g., building drawings) due to the lack of an accurate representation of the existing buildings at the early stage of projects. In addition, these challenges lead to exposing workers into hazard risks which are the main cause to record over 1,000 deaths and 800,000 injuries in the European Union (Rwamamara, Norberg, Olofsson, & Lagerqvist, 2010). Yet to date, all types of building spaces have not been rebuilt as 3D models yet since the labor-intensive, time-consuming and costly process is required. As a result of missing 3D representation of the buildings, especially the aged buildings which undergone multiple renovations and/or remodeling have a high probability of misrepresenting building elements due to the loss of building information and/or omitting the building elements. In this respect, there is a need to develop an efficient and effective way to obtain the geometrical information of building elements in a timely manner (Huber et al., 2011).

An example of these aged buildings that were in dire need for 3D documentation is the Notre Dame Cathedral de Paris as shown in (Figure 1-1-a). The tragic accident of this 850-year-old

23 beautiful structure burning down rendered the world speechless (Figure 1- 1- b) (Eric Levenson,
24 2019). After the accident France’s precedent Emmanuel Macron quickly vowed to rebuild the
25 Notre Dame, moreover, multiple companies announced their support to aid this project (Lyons,
26 2019). A detailed 3D model of the Notre Dame could help speed up the process of drafting,
27 drawing, planning, and construction process. Luckily, the 3D model of the Notre Dame Cathedral
28 was captured by Ubisoft to create a location in their published video game “Assassin creed unity”
29 illustrated in (Figure 1-1-c). The game artists designed the 3D model with immaculate attention
30 to details for the interior and exterior of the building (Gilbert, 2019; Ubisoft, 2019). Another 3D
31 model of the entire structure of the Cathedral is captured extensively in 2010 by Andrew Tallon,
32 an Architectural historian and associate professor of Art at Vassar College using a 3D-laser scanner
33 as shown in (Figure 1-1-d) (Tallon, 2014). These models provide accurate recreation of all the
34 cathedral’s dimensions and surfaces. Notre Dame de Paris is lucky to have these models. However,
35 this is not the case for all historical buildings, that might suffer a similar fate.

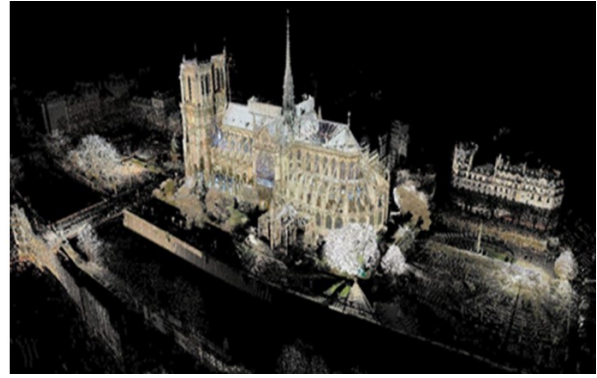


(a)



(b)

36
37
38



39

40

(c)

(d)

41 Figure 1- 1: (a) Notre-Dame de Paris, (b) Tragic accident of the Notre-Dame burning down, (c)
42 Notre-Dame 3D model in Assassins Creed game, and (d) Notre-Dame 3D-PCD (Eric Levenson,
43 2019; Gilbert, 2019; Tallon, 2014; Ubisoft, 2019)

44 3D laser scanner technology attracts the interest of the construction community due to its clear
45 edge over manual or electronic measurement devices in terms of time requirement spent on-site
46 and accuracy (Azhar, Khalfan, & Maqsood, 2012; S. Li, Isele, & Bretthauer, 2008; Wang, Tan, &
47 Mei, 2019). Moreover, its versatility to work under different site conditions such as the levels of
48 lightness and occlusion, the sizes of space areas, and complex space layouts is merit in the
49 construction industry. The aforementioned reasons make the 3D laser scanner the preferred choice
50 for heavily operated buildings (e.g., hospitals) and infrastructures (e.g., tunnels) that are not
51 allowed to stop temporarily or have disturbances for a long period of time (Chida & Masuda, 2016;
52 Wang et al., 2019). The information (e.g., dimensions and locations) of the building elements
53 scanned by the 3D laser scanner is represented by a set of millions of data points formed as X , Y ,
54 Z coordinates in 3D space as shown in Figure 1- 2. As a result, the 3D-point cloud data (3D-PCD)
55 highly represents the detailed 3D geometric information of the as-is state for the surrounding
56 environment of the scanned locations.



57

58

Figure 1- 2: Concordia University EV building Entrance Hall 3D-PCD

59

60

61

62

63

64

65

66

67

68

However, 3D-PCD usually involves: (1) unorganized, noisy and missing data due to occlusion and reflective or transparent surfaces of the building elements; and (2) the large volumes of the files required high computation processing performance to reconstruct accurate as-built 3D models. In this respect, manual processing procedures (also called as a reconstruction phase), which are mostly tedious, error-prone and time-consuming, are needed to develop the 3D building elements and associated properties based on the 3D-PCD. To eliminate these limitations, an automated approach is highly sought from both commercial software and academia (Pătrăucean et al., 2015). However, available commercial software such as CloudCompare and 3DReshaper is not able to identify, segment and reconstruct automatically the building elements such as walls, columns, and stairs yet (3DReshaper, 2019; Compare, 2019). In addition, researchers in the past

69 few years have been successful to reconstruct planar building elements such as walls, ceilings, and
70 floors in single-level spaces based on approaches that involve two steps: 1) identification and
71 segmentation of building elements; and 2) surface reconstruction. At this junction, it should be
72 noted that the main focus of this research is to improve upon the identification and segmentation
73 step, which is still a manual and labor-intensive task with high computation costs, to establish the
74 automated reconstruction process using 3D-PCD. In this respect, previous researchers have
75 introduced different methods of utilizing techniques such as region growing, RANSAC and
76 machine learning algorithms to implement the identification and segmentation step (Chen, Cho, &
77 Kim, 2018; Franz, Irmeler, & Ruppel, 2018; M. Li, Wonka, & Nan, 2016; R. Lu, Brilakis, &
78 Middleton, 2019; Macher, Landes, & Grussenmeyer, 2015, 2017; Murali, Speciale, Oswald, &
79 Pollefeys, 2017; Oesau, Lafarge, & Alliez, 2014; Qi, Su, Mo, & Guibas, 2017; Tatarchenko,
80 Dosovitskiy, & Brox, 2017; Thomson & Boehm, 2015). Based on the previous studies, it has been
81 noted that RANSAC is one of the most commonly used techniques for the identification and
82 segmentation of the building elements for its various benefits such as the ability to be applied for
83 multiple types of the targeted building elements, fast processing time compared to region growing
84 and p-linkage techniques when applied on huge data sets, and easy implementation (M. Li et al.,
85 2016; Murali et al., 2017).

86 **1.2 Problem Statement**

87 Previous approaches suggested by researchers utilizing RANSAC still have the following
88 challenges: (1) RANSAC is inefficiently utilized, due to the arbitrary number of iterations defined
89 by the user leading to the creation of 3D models that misrepresent the as-built conditions due to
90 the over-segmentation, which segments 3D-PCD that do not belong to the building elements, or
91 under-segmentation, which misses 3D-PCD belonging to the building elements; (2) lack of

92 consideration for RANSAC's feature to tend to estimate over or under-estimate the dimensions and
93 orientations of the building elements when it is applied on large datasets; and (3) the proposed
94 methods are limited in applicability since multi-level building spaces such as auditoriums and halls
95 with multiple horizontal building elements are not considered.

96 **1.3 Research Hypothesis**

97 Several questions have arisen in this research hypothesis and they require to be resolved within
98 this research, these questions are as follows:

- 99 1. Is it possible to make RANSAC more efficient? In addition, How?
- 100 2. Is it possible to make RANSAC more accurate and resilient to outliers? Moreover, How?
- 101 3. Is it possible to make the reconstruction of point cloud more flexible to adapt to multi-
102 level rooms?
- 103 4. Can we expand on the reconstructed elements existing in multi-level rooms? If yes,
104 which elements are important? And How?

105 **1.4 Objectives and Scopes**

106 The main objectives of this research are to:

- 107 1. Fully automate the process of identification, segmentation, and reconstruction of the
108 building elements form 3D-PCD.
- 109 2. Improving the efficiency of the utilization of RANSAC.
- 110 3. Reducing errors and enhancing the accuracy of the reconstruction process.
- 111 4. Expanding upon the applicability of the reconstruction process and creating a more
112 accurate representation of the as-built condition, by not only taking into consideration
113 multi-level space but also including more building elements such as columns and stairs.

114 Accordingly, to accomplish these objectives, this research overcomes these challenges and
115 achieves these objectives by the proposed methodology involving the following procedures:

- 116 1. pre-processing to prepare the 3D-PCD by removing outliers and transforming the
117 coordinates of 3D-PCD.
- 118 2. Transformation of the 3D-PCD to 2D images to identify the locations and numbers of
119 the vertical building elements such as columns and walls automatically by implementing
120 Hough circle and line transforms.
- 121 3. Development of standard exploring areas to avoid identifying and segmenting the
122 outliers of 3D-PCD when RANSAC is implemented.
- 123 4. Reconstructing the 3D surface models of the building elements.

124 As a validation, the proposed framework is tested on three cases, a multi-ceilings and columns
125 entrance hall and a multi-floor auditorium with stairs, and the results are analyzed and assessed
126 using an evaluation matrix that composes of seven parameters to evaluate the performances of the
127 proposed method in reconstruction processes of 3D-PCD.

128 **1.5 Expected Contributions**

129 To overcome these limitations, this research proposes an automated reconstruction approach
130 that encompasses the following features:

- 131 1. Automatic identification and segmentation of the building elements with high accuracy
132 and low interference by users;
- 133 2. Competitive computation cost by defining the optimal number of iterations which is
134 used to determine the number of runs for RANSAC.

- 135 3. The standard regions developed based on the building codes to prevent the use of the
 136 outliers and misrepresentation of the building elements during the identification and
 137 segmentation process during the implementation of RANSAC.
- 138 4. Extensibility of the 3D point cloud-based reconstruction process based on the
 139 consideration of the multiple building elements in multi-level building spaces.

140 **1.6 Thesis Organization**

141 Table 1- 1: Titles and summary of each chapter of this Thesis

Chapter Titles	Summary
1. Introduction	This chapter provides the background and a summary of this thesis, also covers the hypothesis, the intended objectives and the expected contribution of this thesis.
2. Literature Review	This chapter discusses the recent studies, algorithms, and methods for each of the main steps of this Thesis.
3. Methodology	This chapter explains the proposed framework to achieve the objectives discussed in the introduction.
4. Implementation	This chapter discusses the equipment used for this framework, the three test cases used to validate the proposed framework, the results, and evaluation for the results.
5. Conclusion	This chapter summarizes the final output of the proposed framework and discusses the future works for it.

142

CHAPTER 2: LITERATURE REVIEW

143

144 This chapter provides a comprehensive review of recent studies and techniques used to
145 automatically identify, segment, and reconstruct building elements from 3D-PCD and their
146 limitations. Reconstruction of 3D point clouds can be categorized mainly by two steps:

147 1. Identification and segmentation of building elements.

148 2. Surface reconstruction.

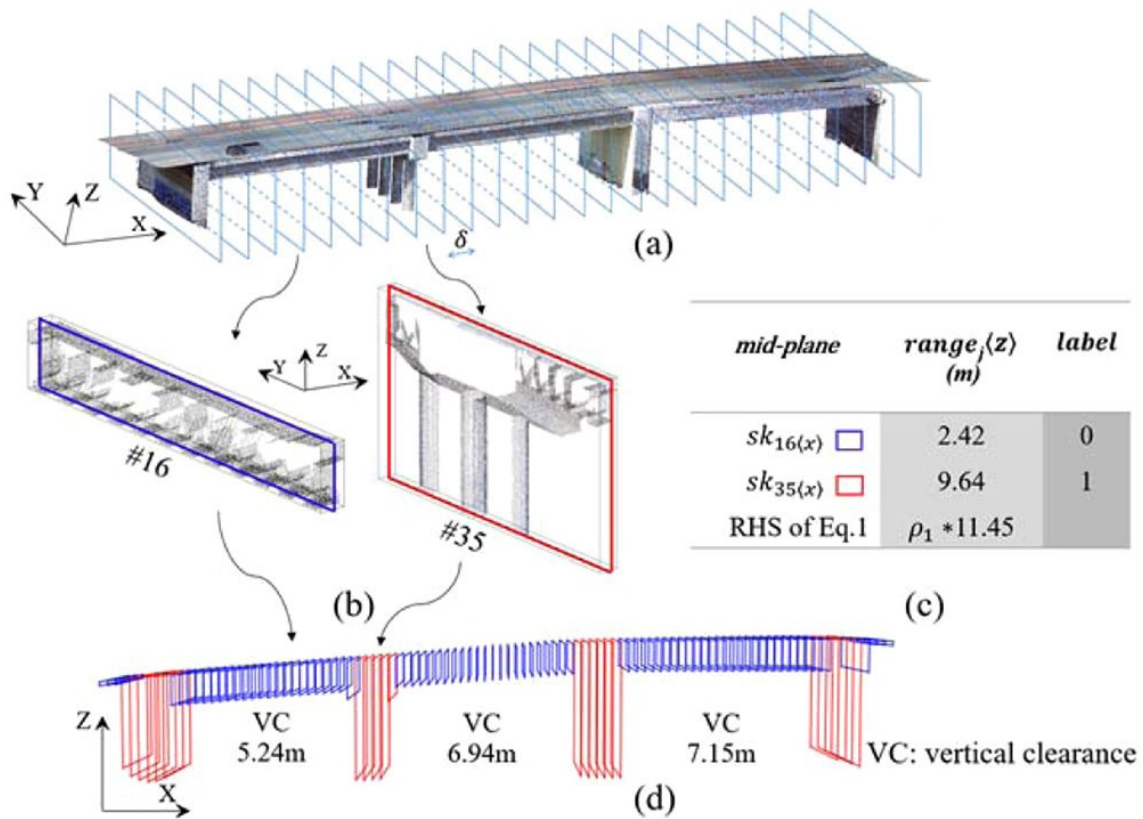
149 Thus, this section discusses the recent studies in both areas to identify the state-of-art in 3D
150 point cloud-based reconstruction. In the end, the research gaps identified will be discussed.

151 **2.1 Identification & Segmentation of Building Elements**

152 Automatic reconstruction of a building's 3D-PCD is a valuable goal sought after by
153 researchers, as the reconstruction process is a manual, tedious, time consuming and error-prone
154 procedure. As discussed earlier the first step for the reconstruction process is the identification and
155 segmentation of these structural building elements such as columns, walls, etc. from the 3D-PCD.
156 In this respect, various techniques were utilized to located and segment these building elements
157 from the 3D-PCD, such as Slices Comparing (R. Lu et al., 2019), Deep Learning (Qi et al., 2017;
158 Tatarchenko et al., 2017), Region Growing (Dimitrov & Golparvar-Fard, 2015), p-linkage (X. Lu
159 et al., 2016), Hough transform (Díaz-Vilariño, Conde, Lagüela, & Lorenzo, 2015), and RANSAC
160 (Schnabel, Wahl, & Klein, 2007). These identification and segmentation techniques can be
161 classified by general methods, feature-based methods, and geometric based methods.

162 2.1.1 General Methods

163 General methods are broad techniques that can be adapted to work for indoor environments. An
 164 example of this method, Lu et al. have introduced a method to identify structural members in
 165 bridges such as columns and slabs. The proposed method is to take multiple slices through the
 166 height of the bridge in both directions (X and Y), compare the heights of the slices to identify the
 167 locations of slabs and piers as shown in Figure 2- 1. Although this method is introduced for the
 168 bridges, this technique could be adopted to identify slabs and columns in one-level rooms (R. Lu
 169 et al., 2019). However, this method is not efficient to identify the slabs and columns in the multi-
 170 level rooms which have various heights of the building spaces since it is difficult to compare the
 171 lengths of the multiple slices.



172

173 Figure 2- 1: Slicing the bridge's 3D-PCD in the X direction (R. Lu et al., 2019)

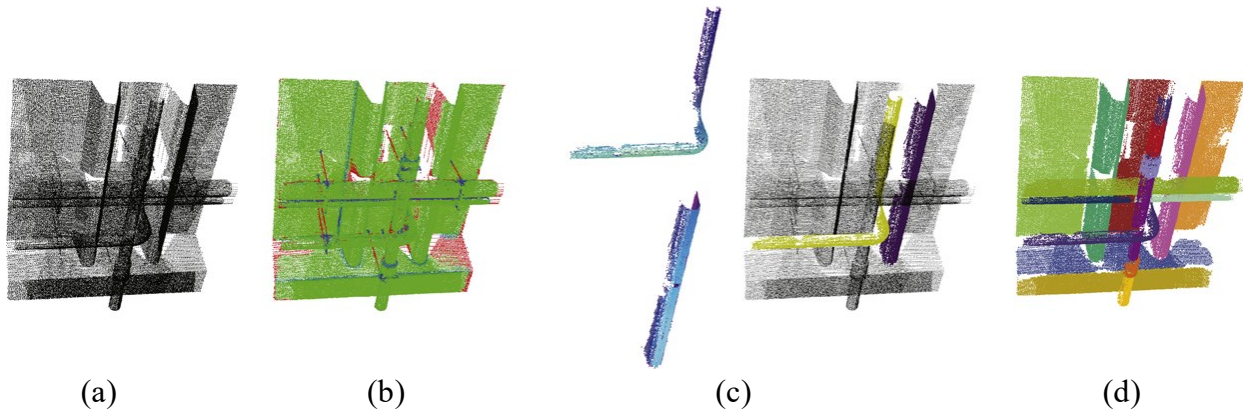
174 Like other efforts, some researchers (Chen, Kira, & Cho, 2019; Qi et al., 2017; Tatarchenko
175 et al., 2017) have used deep learning and neural networks techniques to identify different types of
176 building elements and pieces of furniture from point clouds and voxels acquired in the indoor
177 environment. Although these techniques provide robust and accurate results, they require high
178 computational performance to train the model with large periods of time. Moreover, some of the
179 proposed deep learning techniques suffer from over-segmentation. Furthermore, it is difficult to
180 get annotated data to train the classification algorithm properly. Deep learning is a promising
181 method for the identification and segmentation of building elements from the 3D-PCD since it is
182 quite robust. However, to this point, there is not enough research done to optimize the usage of
183 this method, since 3D-PCDs are large in storage size and require a long time to be annotated to
184 train the models. Moreover, requires high computational time and effort to process.

185 2.1.2 Feature-Based Methods

186 In other efforts, some researchers have turned to feature-based methods. This method assesses
187 some attributes such as surface normal and density of 3D-PCD to identify the building elements.
188 These methods have two popular algorithms, namely Region Growing and p-linkage.

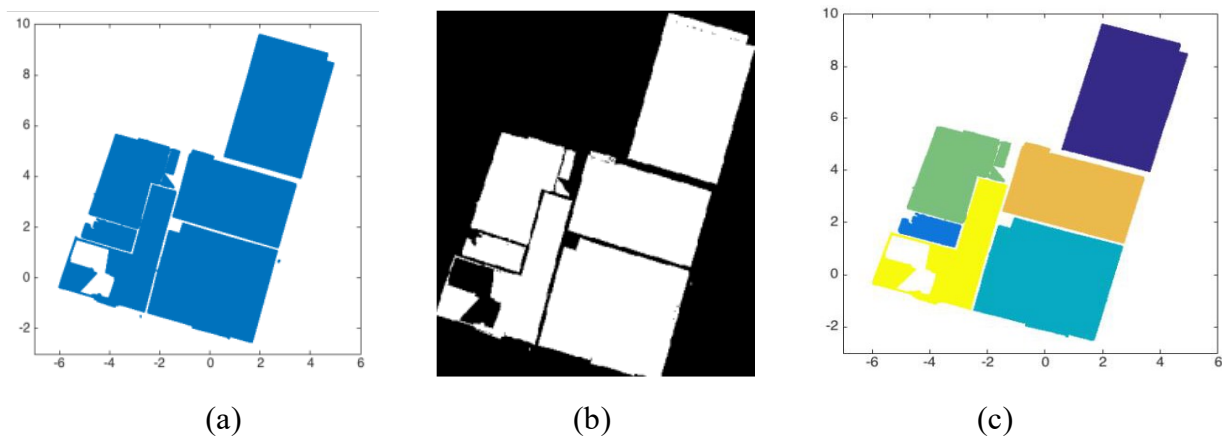
189 Region growing starts selecting one or more points, also called as seed points, which are used
190 to identify the characteristics of the selected points such as normal and curvature. Then, it explores
191 to find the neighbor points which have the same features as ones in the seed points (Grilli, Menna,
192 & Remondino, 2017). Based on this concept, the region growing algorithm is used to not only
193 identify structural members and elements of mechanical, electrical and plumbing (MEP) systems
194 but also segments rooms as the 2D image slices retrieved from the 3D-PCD as shown in Figure 2-
195 2 and Figure 2- 3 respectively (Dimitrov & Golparvar-Fard, 2015; Macher et al., 2015). On the
196 other hand, p-linkage is a novel clustering algorithm that behaves similarly to the region growing

197 algorithm but considers the densities of the point clouds instead of the features of the points (X.
198 Lu et al., 2016).



199
200 (a) (b) (c) (d)

201 Figure 2- 2: (a) Point Cloud, (b) Feature detection, (c) Region growing, and (d) Final
202 segmentation (Dimitrov & Golparvar-Fard, 2015)



203
204 (a) (b) (c)

205 Figure 2- 3: (a) Slice from the 3D-PCD at ceiling level, (b) generating the image, and (c) Region
206 growing output (Macher et al., 2015)

207 However, these techniques may have lower accuracy and efficiency than other techniques
208 since they tend to not only use the outliers leading to segment the wrong 3D-PCD called over-
209 segmentation but also miss the data related to the building elements called as under-segmentation.

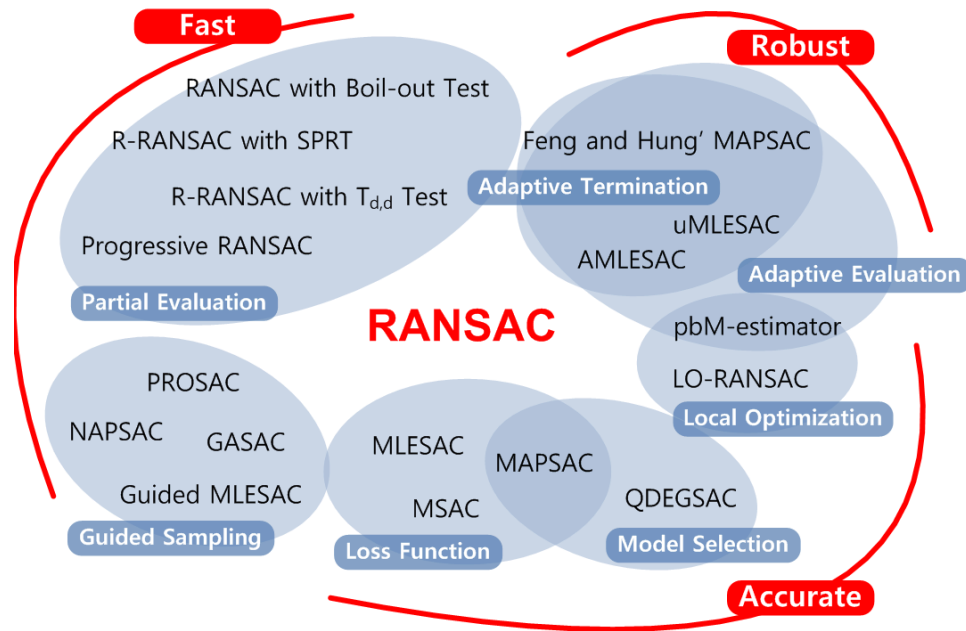
210 In addition, both algorithms require high computational costs in terms of performance and time
211 when the feature-based methods are applied using a high volume of the point cloud data.

212 2.1.3 Geometry-Based Methods

213 Another approach explored by researchers is geometry-based methods. In comparison to the
214 other two methods, this method usually exhibits the lowest computational time and most
215 commonly used, therefore, it is the base for this research's suggested framework. Since, almost all
216 building elements (e.g., walls and columns) boil down to simple geometrical shapes consisting of
217 planes and cylinders in 3D space or lines and circles in 2D space, researchers utilized this concept
218 to locate the building elements (Chen et al., 2018). Previous works have used mainly Hough
219 transform and RANSAC to identify the geometrical shapes of building elements in either 2D or
220 3D space. Hough transform is a feature extraction method to find specific shapes such as circles,
221 ellipses and lines and their locations on the 2D images in computer vision and image processing
222 (Díaz-Vilariño et al., 2015). Furthermore, the Hough transform detects multiple building elements
223 in a single run without the influences of the occlusion (Grilli et al., 2017). Based on these benefits,
224 researchers have expanded the utilization of Hough transform which is to identify the locations of
225 building elements (Díaz-Vilariño et al., 2015; Oesau et al., 2014).

226 RANSAC algorithm is an iterative technique used by researchers for the segmentation of
227 building elements (i.e., walls) from the 3D-PCD based on the following procedures: (1) select
228 subsets of points randomly associated with a building element from the 3D-PCD; (2) attempt
229 iteratively to fit a 3D model such as planes or cylinders into the selected subset data; and (3) detect
230 the outlier points that do not fit the model and remove them from the selected subset data.
231 RANSAC has many descendants such as MILESAC and AMILESAC. Some of the descendants
232 have improved the accuracy and others focus mainly on improving the robustness of RANSAC as

233 shown in Figure 2- 4 (Anagnostopoulos, Pătrăucean, Brilakis, & Vela, 2016; Choi, Kim, & Yu,
 234 1997; Grilli et al., 2017; Hong et al., 2015; Jung et al., 2014; Tarsha-Kurdi, Landes, &
 235 Grussenmeyer, 2007).



236
 237 Figure 2- 4: RANSAC family (Choi et al., 1997)

238 To address this limitation, previous researchers have introduced RANSAC-based methods
 239 with the Manhattan world assumption, in which all building elements are orthogonal to each other.
 240 In this respect, RANSAC is used as one of the steps to extract as many plane surfaces as possible
 241 that are perpendicular to each other (M. Li et al., 2016; Murali et al., 2017). As a result, this
 242 assumption reduces not only the computational time but also the viability of the proposed methods
 243 since not all building elements are perpendicular to each other (Delage, Lee, & Ng, 2007;
 244 Furukawa, Curless, Seitz, & Szeliski, 2009). In an effort to increase the viability and robustness
 245 of RANSAC, some researchers do not adhere to the Manhattan World assumption. These efforts
 246 utilized RANSAC or one of its descendants in a similar approach to the aforementioned method
 247 by giving them numerous iterations to detect as many walls, ceilings, and floors, as possible

248 without adhering to a specific orientation. this approach detects elements that are not orthogonal
249 to each other, however, these approaches are more time consuming (Macher et al., 2015, 2017;
250 Ochmann, Vock, & Klein, 2019; Schnabel et al., 2007; Thomson & Boehm, 2015).

251 It is clear that the utilization of RANSAC so far still has some limitations such as: (1) the
252 arbitrary number of iterations, which not only leads to the inefficient implementation of RANSAC
253 in terms of computational time and performance but also, might lead to over or under
254 segmentation; (2) RANSAC is affected by false data causing segmenting false 3D-PCD that do
255 not belong to the targeted building element when applied in large 3D-PCD; and (3) inability to fit
256 multiple types of 3D models such as cylinders and planes at the same time (Pérez-Sinticala et al.,
257 2019; Tarsha-Kurdi et al., 2007; Zhang, Huang, Zhang, & Luo, 2017). It should be noted that,
258 based on the benefits exhibited by Hough transform and RANSAC, this research suggests a
259 procedure that uses a Hough transform, Region of interest (ROI) and RANSAC in a manner to
260 overcome RANSACS limitations mentioned earlier.

261 **2.2 Surface Reconstruction**

262 Surface reconstruction of building elements 3D-PCD is the second step for the automatic
263 reconstruction of 3D-PCD. It is the creation of smooth surfaces and shapes that have the same size
264 and location as the building element found in the point cloud (Berger et al., 2017). There are
265 various efforts introduced in recent years to reconstruct indoor environments either after the
266 segmentation step of the point cloud or straight forward from the original point cloud. Oesau et al.
267 (Oesau et al., 2014) partitioned the bounding box of the 3D-PCD into volumetric cells and labeled
268 these cells either full or empty spaces based on the locations of the building elements. Next, the
269 reconstructed model is developed from these labeled volumetric cells. As a different effort,
270 Thomson et al. (Thomson & Boehm, 2015) proposed a method in which relevant points that

271 represent the coordinates of the boundaries are collected, and used to reconstruct walls, ceilings
272 and floors. The second method is the reverse of the aforementioned method. This method loads
273 objects bounding boxes to the memory, then use these bounding boxes to reconstruct the point
274 cloud. On the other hand, Macher et al. (Macher et al., 2017) exported the planes that represent
275 walls, ceilings, and floors to OBJ format. Similarly to Oesau et al., Murali et al. (Murali et al.,
276 2017) used information gathered from the segmentation step to fit cuboids that represent rooms
277 and find connections between them and cluster them together. Recently, Franz et al. (Franz et al.,
278 2018) suggested a novel method to reconstruct point cloud in real-time. The processing is done on
279 the 2D horizontal section of the point cloud. The reconstruction process of the outer and inner
280 walls takes place by using boundaries gathered from 2D horizontal sections.

281 **2.3 Research gaps and objectives**

282 The automatic reconstruction of 3D-PCD is supposed to improve efficiency, cost-
283 effectiveness and reduces the time compared to manual processing. Therefore, it has been the
284 interest of many researchers to study this area. However, on the basis of the literature review, and
285 to the best knowledge of the author, previous studies still need to be improved due to the following
286 challenges: (1) manual tasks with high computation cost and error-prone in identification and
287 segmentation process since RANSC is implemented by a random number of runs determined by
288 users or a large number of experiences which may lead to failure to segment 3D-PCD belonging
289 to the building elements by either over-segmenting the 3D-PCD or under-segmenting it; (2) a lack
290 of considering a feature of RANSAC which tends to estimate over-or under-estimate dimensions
291 and orientations of the building elements when it explores to identify and segment 3D-PCD of the
292 building element in large areas; and (3) the lack of applicability in 3D reconstruction process for

293 multiple-level building spaces involving ceilings, floors, and stairs corresponding to the as-built
294 conditions.

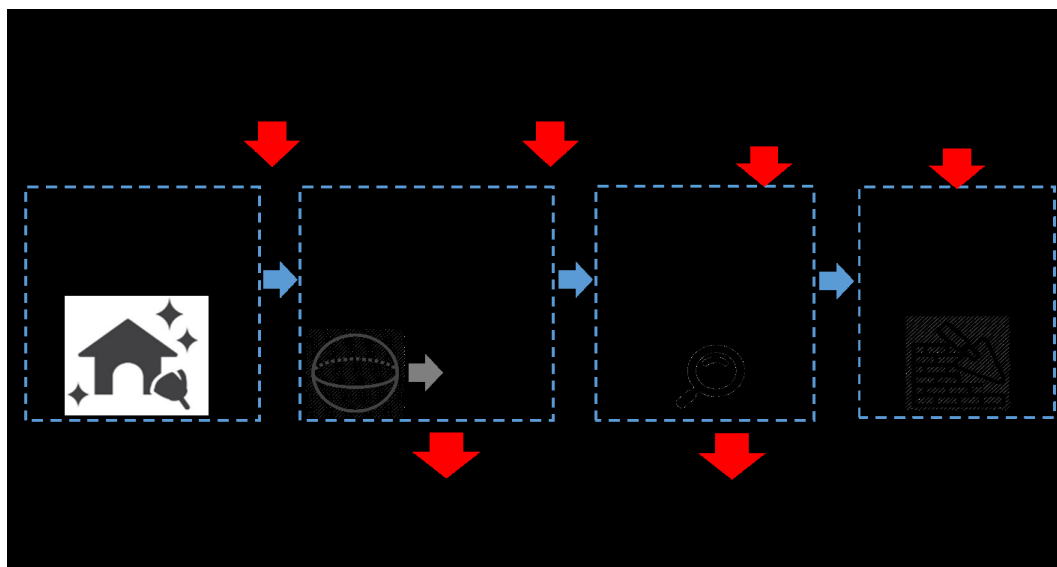
295 Accordingly, this research study aims to overcome these challenges and fill these gaps by
296 proposing a framework to automatically identify, segment and reconstruct building elements from
297 3D-PCD. The objectives are achieved by the proposed methodology which can improve upon the
298 efficiency of utilization of RANSAC by specifying the number of iterations instead of being given
299 an arbitrary number of iterations. Moreover, the proposed method reduces the effect of outliers on
300 RANSAC by specifying locations and areas where RANAC will be utilized, which leads to a
301 reduction in errors and an improvement to accuracy. Finally, widen the scope of applicability of
302 the reconstruction process by adding more building elements such as stairs and columns, and
303 considering multi-level space such as cinemas and auditoriums with multi-ceiling and/or floors,
304 creating a more accurate representation for the as-built conditions.

305

306

CHAPTER 3: METHODOLOGY

307 This chapter describes the proposed method to automatically identify, segment and reconstruct
308 the building elements from the 3D-PCD. Figure 3-1 presents the suggested framework, and the
309 evaluation approaches used for the output. The framework consists of the following four steps: (1)
310 pre-processing as 3D point cloud preparation; (2) transforming 3D point cloud to 2D image
311 preparing for vertical building elements identification; (3) identification and segmentation of the
312 building elements; and (4) surface reconstruction to develop a 3D model adopted by multiple
313 software. It should be noted that the proposed method is fully automated after the Pre-processing
314 step. The input of the proposed framework is the 3D-PCD obtained by multiple scans which are
315 implemented by a 3D laser scanner to reduce the blind spots and increase the accuracy of 3D-PCD.
316 The framework is developed in MATLAB and CloudCompare(Compare, 2019; The Math Works,
317 2019) to reconstruct a 3D model that can be adopted into Revit. To evaluate the proposed
318 framework, the evaluation matrix including accuracy, difference, recall, deviation, processing
319 time, precession and F1 score is developed and applied.



320

321

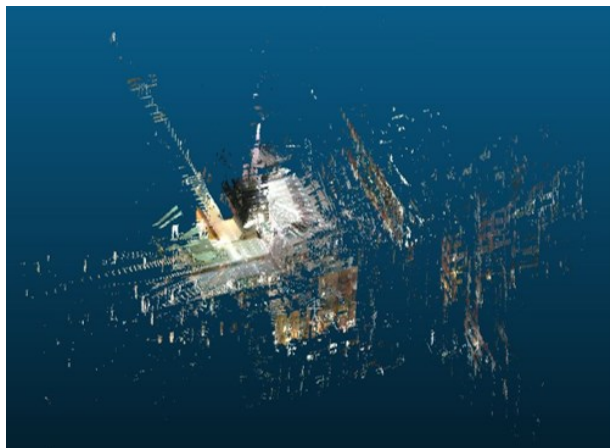
Figure 3- 1: An overview of the proposed methodology

322 3.1 Pre-processing

323 The objective of the pre-processing in this research is to ensure that 3D-PCD has sufficient
324 quality before the transformation, Identification and segmentation, and surface reconstruction. In
325 this respect, the targets of this step are: (1) prevention of blind spots; (2) outlier removal; and (3)
326 3D-PCD leveling. It is important for the proposed method to capture building elements by multiple
327 scans on different locations of the observation space (i.e., room) to not only ensure all sides of
328 vertical building elements (e.g., columns) are visible but also minimize the loss of 3D-PCD. In this
329 respect, the multiple scans are conducted and their 3D-PCD are combined using Trimble
330 RealWorks 10.0 (Trimble, 2019) which is software associated with the 3D scanner used. Although
331 the combination of multiple scans provides better quality of 3D-PCD, the other aspect of this work
332 is to generate a large volume of the 3D-PCD size which leads to increase the processing time with
333 the low computational performance. Therefore, it is necessary to downsize and clean the 3D-PCD
334 by manual intervention using CloudCompare. The reduction of 3D-PCD size is achieved by sub-
335 sampling the 3D-PCD randomly and outlier removal. The subsampling is accomplished by
336 CloudCompare arbitrarily picking a specified number of points from the 3D-PCD, this number is
337 defined by the user based on the processing capabilities of the user's computing device. However,
338 the number defined by the user should not be too low that it affects the quality of the 3D-PCD
339 causing data loss and reduction in the accuracy of the proposed method.

340 The existence of reflective or transparent objects such as windows and mirrors generally
341 produce the outliers and false data in 3D-PCD which causes a reduction in the accuracy of the
342 proposed method, especially in the identification and segmentation of building elements step.
343 Removing the outliers caused by these transparent surfaces is done manually by trimming the
344 bounding box to get only the 3D-PCD of the observation space based on visual inspection. Outlier

345 detection was done manually through visual inspections. Figure 3-2 illustrates the 3D point cloud
346 data before and after removing outliers. For successful transformation 3D-PCD to a 2D image, the
347 coordinate transformation is implemented to identify the suitable dimension (length and width) of
348 the 2D image which is determined by calculating the differences between the highest and lowest
349 points in 3D-PCD. After filtering the 3D-PCD by removing the outlier, leveling it might be needed
350 to ensure that the vertical elements are not tilted. This is to ensure the vertical elements are visible
351 in the 2D images in the upcoming step. The leveling of the 3D-PCD is done manually utilizing
352 CloudCompare, by defining three points on the surface by the user and cloud compare will use a
353 transformation matrix to change the coordinates of the 3D-PCD. At this junction, it should be noted
354 that the loss of 3D-PCD may occur when the suitable dimension of the 2D image is not designed
355 since the 3D-PCD is projected to the 2D image in the transformation process. Furthermore, to
356 reduce the computational times for the transformation process, the X , Y , and Z coordinates of the
357 3D-PCD are required to move into the positive region in the three-dimensional space so that all of
358 the coordinates have positive values.



(a) Before removing outliers

(b) After removing outliers

Figure 3- 2: 3D-point cloud data

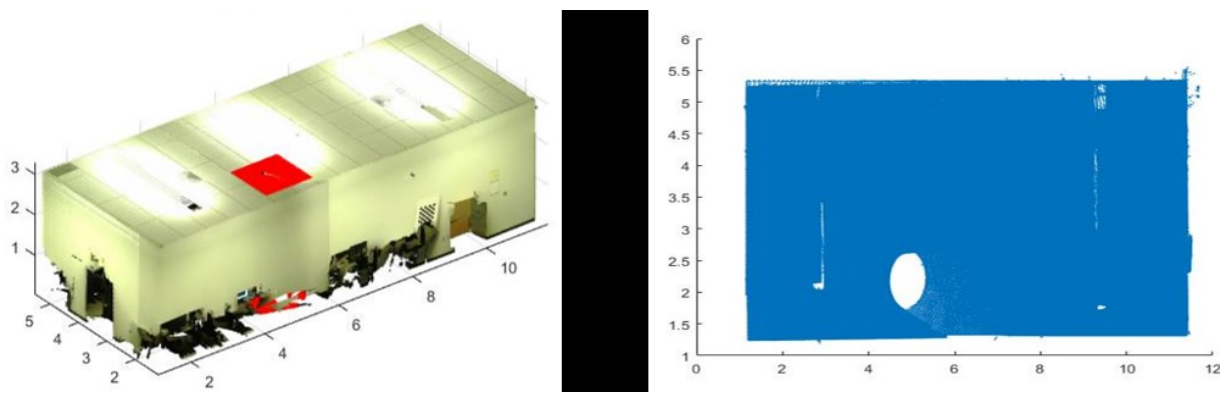
362 3.2 Transforming 3D point cloud to 2D image

363 After pre-processing, 3D-PCD is required to transform into a 2D image which is an essential
364 input to identify and segmentation of the vertical elements (e.g., columns and walls). For the
365 successful transformation and column segmentation, this research uses a method proposed by
366 Vilarino et al. (Díaz-Vilariño et al., 2015) since it provides high accuracy and time-efficiency.
367 However, previous research proposed the method to identify and segment only the columns. In
368 this respect, this research needs to modify the selected method to improve the extensibility which
369 is required to identify all of the vertical building elements. As illustrated in as shown in Figure 3-
370 3, the transformation of 3D-PCD into the 2D image has the following procedures: (1) project 3D-
371 PCD on a 2D plane; (2) apply threshold and binary; and (3) conduct canny edge detection (Ding
372 & Goshtasby, 2001).

373 To project 3D-PCD on a 2D plane with short computational time based on preventing the loss
374 of the data, proper width and height of the 2D plane are determined by identifying and calculating
375 the differences between the maximum and minimum values of the X and Y coordinates. As shown
376 in (Figure 3-3-b), 3D-PCD is projected on the 2D plane, also called as the histogram including a
377 number of points at each pixel, after eliminating Z values of the points. Since all of the points,
378 which represent vertical and horizontal building elements, are projected on the 2D plane, some
379 pixels including vertical building elements have a large number of points compared to other pixels
380 that involve the horizontal building elements such as floors and ceiling. Since the objective of
381 transforming 3D-PCD into the 2D image is to identify the vertical building elements, the points
382 related to the horizontal building elements must be removed from the 2D image. In this respect, a
383 threshold depending on the size of 3D-PCD is defined by 30 points for small spaces such as the
384 rooms, labs, washroom and 60 points for large areas such as entire houses and office buildings.

385 These thresholds are determined based on the experiments in this paper. That is, when the number
386 of points at the pixels is less than the threshold, the number of points is defined as zero to remove
387 the undesired building elements from the 2D image. Otherwise, as shown in (Figure 3-3-c), the
388 number of points at the pixels is not changed and these pixels are considered as the vertical building
389 elements which are columns represented as circles and walls represented as the straight lines. To
390 illustrate the vertical building elements clearly in the 2D image for the shape identification
391 algorithm (i.e., Hough Transform), an edge detection technique such as Canny, Prewitt, Roberts,
392 and Sobel should be implemented to extract, smoothen and filter the edges in the binary image. In
393 this respect, the 2D image is converted as a binary image which the white pixels regard as potential
394 vertical elements and black pixels are the locations of no interest objects. At this junction, it should
395 be noted that the canny edge detection technique provides the smoothest, single-pixel thickness
396 and well-connected edges for lines and circles based on the experiments in this paper. Furthermore,
397 the Canny edge detector is the best technique to collaborate with circle and line Hough transform
398 in terms of accuracy of the shape identification. As shown in (Figure 3-3-d), the Canny edge
399 detector produces the smooth 2D image by removing the noise using a Gaussian filter and fixing
400 and improving the edges using a hysteresis threshold. More details could be found in Vilarino et
401 al. (Díaz-Vilariño et al., 2015).

402

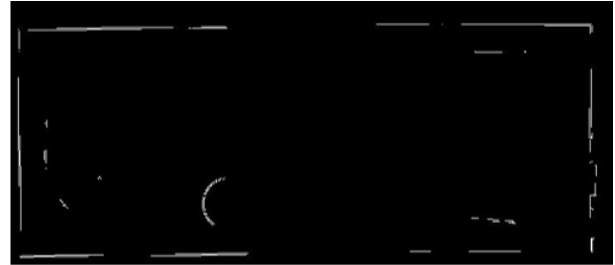
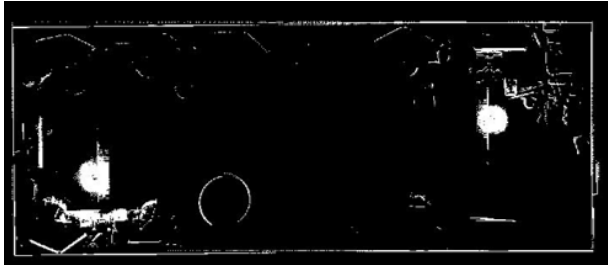


403

(a)

(b)

404



405

406

(c)

(d)

407 Figure 3- 3: (a) 3D point cloud, (b) Projecting the 3D point cloud on a 2D plane, (c) Canny edge
408 detection, and (d) Threshold and Binary

409 3.3 Identification and segmentation

410 The identification and segmentation are implemented based on the types of building elements
411 which are horizontal and vertical elements. Furthermore, preliminary surfaces of segmented
412 building elements are developed as a pre-requisition step for 3D model reconstruction. At this
413 junction, it should be noted that to complete the identification and segmentation successfully, this
414 research adopts a few algorithms: (1) Hough circle and line transform to identify vertical building
415 elements, such as columns and walls; and (2) RANSAC cylinder and plane to not only identify
416 and segment vertical and horizontal building elements such as walls, floors, and ceilings but also
417 develop preliminary surface models for all types of building elements. In this respect, the main
418 resources for this step are the 2D images for the identification of the vertical building elements
419 and 3D-PCD for the segmentation of the building elements.

420 3.3.1 Vertical Plane Building Elements

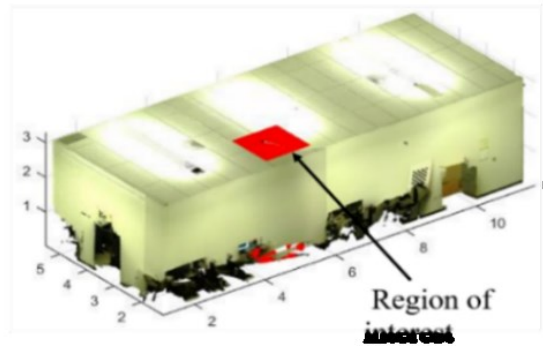
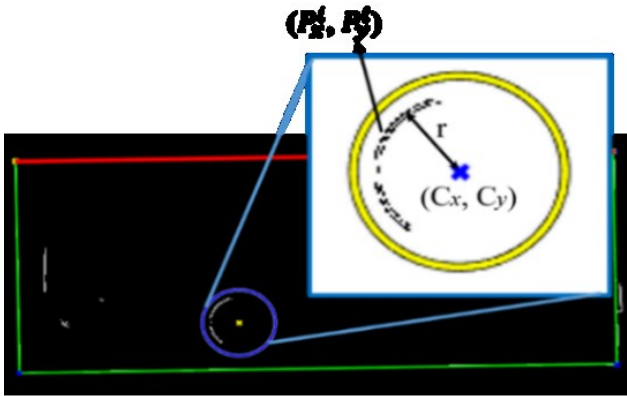
421 Based on the 2D image, Hough circle transform (HCT) identifies the column information
422 including locations, number of columns, and radii from the 2D image. In terms of radii
423 computation for columns, HCT assumes the radii as the range of 9 to 50 cm since circular concrete
424 columns usually have radii of 10 cm or more (Giakoumelis & Lam, 2004). Since all points on the
425 2D image are represented as X and Y coordinates, as shown in (Figure 3- 4- a), the radius (r_j),
426 which is j th of the columns, is computed by the following procedures: (1) identify the center of the
427 circle (C_x, C_y); (2) calculate the distances between (C_x, C_y) and the points (P_x^i, P_y^i); and (3) select
428 the maximum value among the distances resulted by the step (2). Based on these procedures, the
429 radii of the identified columns are determined satisfying Eq. (1). The number of columns is
430 determined by the number of circles found by the HCT in the 2D image.

$$431 \quad r_j = \text{Max}[\sqrt{((P_x^i - C_x)^2 + (P_y^i - C_y)^2)}] \quad i = 1, 2 \quad j=1, 2 \quad (1)$$

432 Where i = a number of points in j th of columns; j = a number of columns.

433 As a conservative process to prevent the loss of 3D-PCD, the region of interest (ROI) is defined
434 as the structures located within a rectangular box centered on the center of the column, the length
435 (L_{ROI}) and width (W_{ROI}) of which are made 3D PCD-specific according to the relationship, L_{ROI} ,
436 $W_{ROI} = (1.3 \times 2 \times r_j)$ (Figure 3- 4- b). Once the locations, ROIs, and the number of columns is
437 identified by HCT, this information projects into 3D-PCD for the segmentation of the columns.
438 However, as shown in (Figure 3- 4- c), the segmented column has an uncompleted shape of the
439 column which may lead to failing 3D model reconstruction. In this respect, the surface models
440 illustrated in (Figure 3- 4- d), which are used as input for 3D model reconstruction is fitted utilizing
441 cylinder RANSAC, are developed to recover uncompleted parts of the columns. It should be noted

442 that the height of the column is determined by measuring the distance between the maximum and
443 minimum of Z coordinates on the ROI in 3D-PCD.



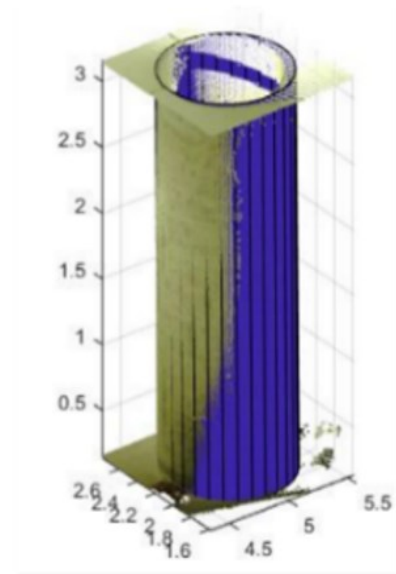
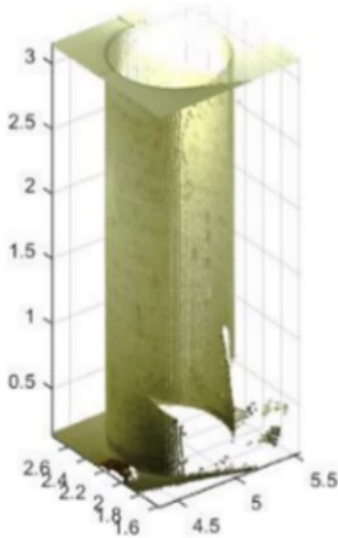
444

445

(a)

(b)

Column #1



446

447

(c)

(d)

448

Figure 3- 4: Identification and segmentation of a column

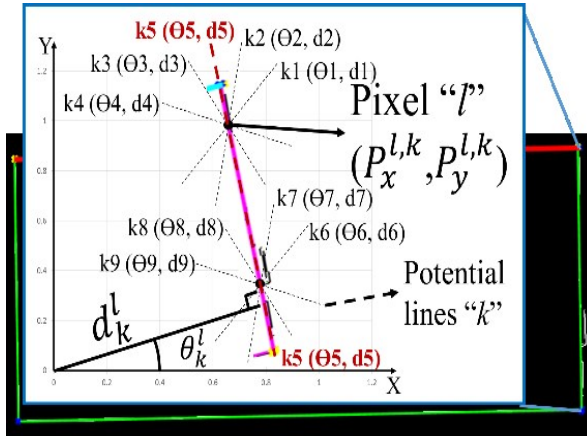
449 As a continuous work to reconstruct the vertical plane elements in the building, Hough line
450 transform (HLT) is used to identify wall information such as the locations, lengths, and the number
451 of lines in the 2D image. In terms of lengths and the number of lines for walls, HLT assumes that

452 the lengths of the walls should be at least 100 cm as a conservative measure since the minimum
453 wall length in rooms (bathrooms) should not be less than 120 cm in the building code in Ontario
454 (Giakoumelis & Lam, 2004). Since all points on the 2D image are represented as X and Y
455 coordinates, as shown in (Figure 3- 5- a), the number and lengths of the lines are computed by the
456 following procedures: (1) calculate the distances (d_k^l) using Eq. (2) from the origin point (0, 0) to
457 the closest points ($p_x^{l,k}, p_y^{l,k}$) on potential lines (k) generated by angles (θ_k^l), which is a range [-90,
458 90]. The potential lines must pass through pixels (l) located on a wall line; (2) map d_k^l and θ_k^l on
459 2D graph which x-and y-axis are θ and d , respectively; and (3) identify the points which have the
460 same values of the θ and d . These points become wall lines that are used to determine the number,
461 locations, and lengths of walls.

$$462 \quad d_k^l = p_x^{l,k} \cos\theta_k^l + p_y^{l,k} \sin\theta_k^l \quad (2)$$

463 Unlike the segmentation of columns, the identified walls are segmented by utilizing plane
464 RANSAC algorithm instead of ROI to prevent to involve outliers and false data such as furniture
465 into the wall dataset. However, one of the shortcomings commonly associated with using
466 RANSAC is the arbitrary number of iterations for RANSAC given by the users, this might cause
467 over or under segmentation of the given data leading to wastage of computational effort and time.
468 Therefore, this research overcomes these issues by defining the number of iterations of RANSAC
469 as the number of walls identified from HLT. RANSAC segments the 3D-PCD of walls based on
470 the following procedures: (1) randomly selecting a subset of points of the 3D-PCD; (2) fitting a
471 vertical plane model in the selected subset; (3) finding the number of inliers and outliers of the
472 plane model based on a threshold defined by the user equal to 0.04 cm; (4) repeating the previous
473 steps till finding the plane model with the most inliers. Once the vertical plane models with most
474 inliers are located by RANSAC illustrated in (Figure 3- 5- b), the inlier points are segmented and

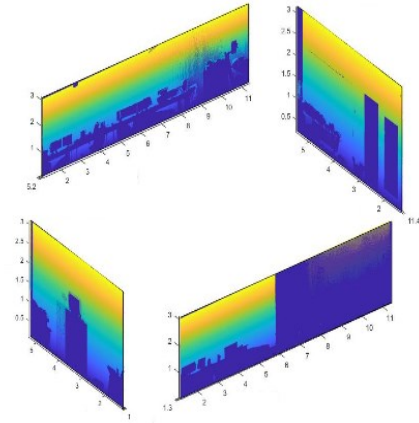
475 labeled as walls represented in (Figure 3- 5- c). Information about the dimensions of the segmented
 476 walls and their plane models are used not only to identify the ceiling, floors, and stairs but also in
 477 surface reconstruction steps.



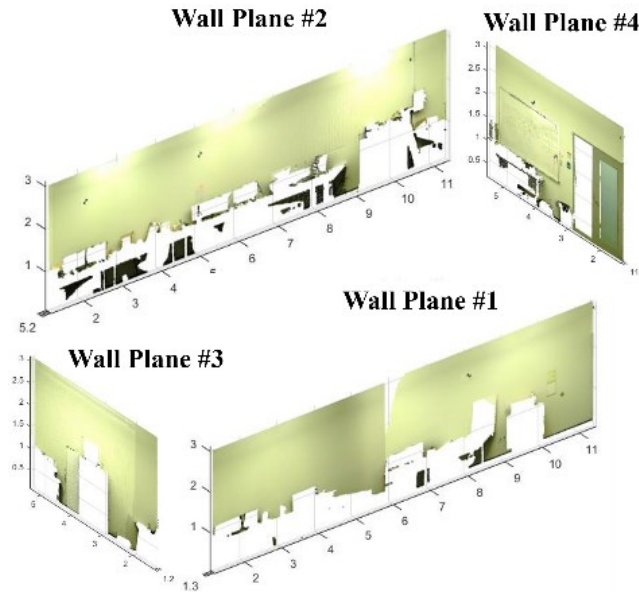
478

479

(a)



(b)



480

481

(c)

482

Figure 3- 5: Identification and segmentation of walls

483

484 3.3.2 Horizontal Plane Building Elements

485 For the identification and segmentation process of horizontal plane elements such as ceilings,
486 floors, and stairs, this research uses a heuristic approach which implements plane RANSAC
487 iteratively in the ROIs defined in the 3D-PCD. The proposed heuristic approach is implemented
488 by the following procedures: (1) the heights of the walls segmented in the previous step are
489 identified and compared; (2) when there are different heights on the walls, there are multiple floors
490 and connected by stairs; (3) the wall with the lowest height is used as a datum for defining the
491 ROIs of the horizontal plane elements; (4) the ROIs are subdivided into sub-ROIS, the sizes of the
492 sub-ROIs are determined based on the height of the ROI and the type of the horizontal plane
493 elements; (5) horizontal and vertical plane RANSAC is utilized in each sub-ROI to identify,
494 segment and create preliminary surface for the horizontal plane elements in it; and (6) the x, y, z
495 coordinates of the segmented 3D-PCD are compared in each iteration of RANSAC to the
496 predecessor iteration to eliminate the repeated 3D-PCD which have the same values of the
497 coordinates.

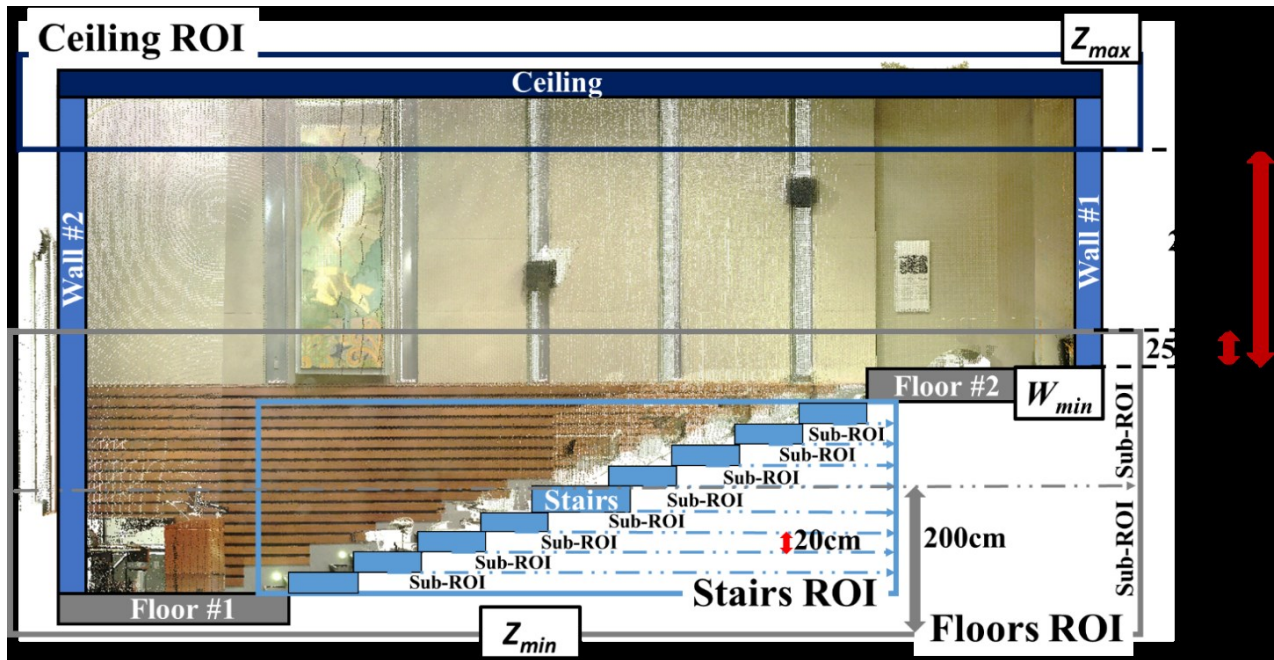
498 The ROI is the area where the targeted horizontal plane elements may exist in the 3D-PCD.
499 In this respect, according to the types of horizontal building elements, defining these ROIs is
500 crucial to not only improve the accuracy but also reduce the computation times in the identification
501 process. The ROIs are determined based on the types of the horizontal plane elements, Z-
502 coordinates of the 3D-PCD, and the logical locations of the building elements. For example, the
503 floors are logically located in the lowest level of the building and connected to the bottom of the
504 walls. Therefore, the ROI of the floors is defined from the minimum Z coordinate (Z_{min}) of the 3D-
505 PCD to the lowest Z coordinate (W_{min}) among the walls adding 25 cm. At this junction, it should
506 be noted that this research uses 25 cm for a safety measure. To identify potential locations of the

507 ceilings in the 3D-PCD, the ROI is defined from 200 cm above the W_{min} to the highest Z coordinate
508 (Z_{max}) among the 3D-PCD. This research uses 200 cm as the starting level for the identification of
509 the ceilings to satisfy the following requirements: (1) the minimum height of a room which is 210
510 cm in the building code, Ontario in Canada (ONTARIO, 2017); and (2) a conservative process to
511 prevent the loss of the 3D-PCD. At this junction, it should be noted that the ROIs of the ceilings
512 and floors are defined by a location of a wall, which is the lowest height among the walls
513 segmented by the previous step in order to ensure the robustness of the proposed method in the
514 multiple-level building spaces. In addition, comparing the heights of walls provides whether there
515 are multiple floors in the building space or not. For instance, the proposed method considers that
516 there are multiple floors in the space which requires the stairs to allow people to access to the
517 floors when the heights of the walls are different. Depending on the number of different wall
518 heights, the number of floors is determined. That is, as shown in (Figure 3- 6- a), the proposed
519 method compares the heights of the walls and identifies that there are two different wall heights.
520 Due to these different wall heights, this space requires two floors and one staircase to build one
521 single space.

522 Based on this information, the staircase ROI is defined between these two floors. However, in
523 the multi-level building cases, the ROIs are generally large areas involving multiple ceilings and/or
524 floors which lead to not only reduce the accuracy but also increase the computation times in the
525 reconstruction process since the RANSAC tends to identify and segment the incorrect horizontal
526 plane elements using outliers and false 3D-PCD which are not parts of the target horizontal
527 building elements. To address this limitation for the accuracy improvement and the reduction of
528 the computation times, this research divides these ROIs into sub-ROIs to reduce the area in which
529 the horizontal plane RANSAC is applied to identify and segment the multiple ceilings and floors.

530 These sub-ROIs are defined using an interval that is 200cm for the ceiling and floors based on the
531 number of experiments implemented by authors. At this junction, it should be noted that the sub-
532 ROIs are not necessary when the ROI dimension (e.g., heights and lengths) is less than 200cm. On
533 the other hand, the interval for the staircase sub-ROI is 20 cm which is determined based on the
534 maximum height of the rise in the building code, Ontario (ONTARIO, 2017).

535 Horizontal plane RANSAC is implemented at each of the sub-ROIs to identify, segment and
536 construct the preliminary surfaces of the ceilings and floors. In the case of stairs, horizontal and
537 vertical plane RANSAC are used to identify, segment and construct the preliminary surfaces of
538 the stairs including the run and rise components. However, this heuristic approach might segment
539 the same 3D-PCD multiple times during the iterations when the ceiling and floors 3D-PCD are
540 located in the multiple sub-ROIs. To prevent this multiple uses, the proposed method compares
541 the x , y , and z coordinates among the 3D-PCD identified and segmented by plane RANSAC at
542 each of the sub-ROIs in order to ensure the only one single use of the 3D-PCD by eliminating the
543 other 3D-PCD which has the same values of the coordinates. Identification and segmentation of
544 the horizontal building elements such as floors, ceilings, and stairs provide the following outputs:
545 (1) the segmented 3D-PCD; (2) plane models which are mainly used in the reconstruction process;
546 and (3) the region between the multiple floors in one single space to identify the stairs rise and run.
547 As a result, the process flow of identifying and segmenting the horizontal building elements is
548 described as the pseudo-code presented in (Figure 3- 6- b).



549
550

(a)

```

A: Original 3D-PCD
Wmin: Min (Z-coordinates of walls)
Zmax = Max (Z-coordinate of A)
Zmin = Min (Z-coordinate of A)
C = [ ] /* Empty list for surface models of ceilings */
F = [ ] /* Empty list for surface models of floors */
S = [ ] /* Empty list for surface models of stairs */
IF the identification and segmentation of ceilings
  FOR R=( Wmin +200cm) to Zmax:
    CeilingExploring = R + 200cm
    If CeilingExploring ≠ Zmax
      Implement RANSAC planes horizontally between R and CeilingExploring
      Develop the surface model of ceiling (SPC)
      Append SPC to C
  Elseif the identification and segmentation of floors
    FOR Zmin to ( Wmin +25cm):
      FloorExploring = Zmin + 200cm
      If FloorExploring ≠ ( Wmin +25cm)
        Implement RANSAC planes horizontally between Zmin and FloorExploring
        Develop the surface model of floor (SPF)
        Append SPF to F
  Elseif a number of different wall heights > 1 for the identification and segmentation of stairs
    Fmin = Min (Z-coordinates of F)
    Fmax = Max (Z-coordinates of F)
    FOR Fmin to Fmax
      StairsExploring = Fmin +20cm
      If StairsExploring ≠ Fmax
        Implement RANSAC planes vertically and horizontally between Fmin and StairsExploring
        Develop the surface model of the stair (SPS)
        Append SPS to S
END

```

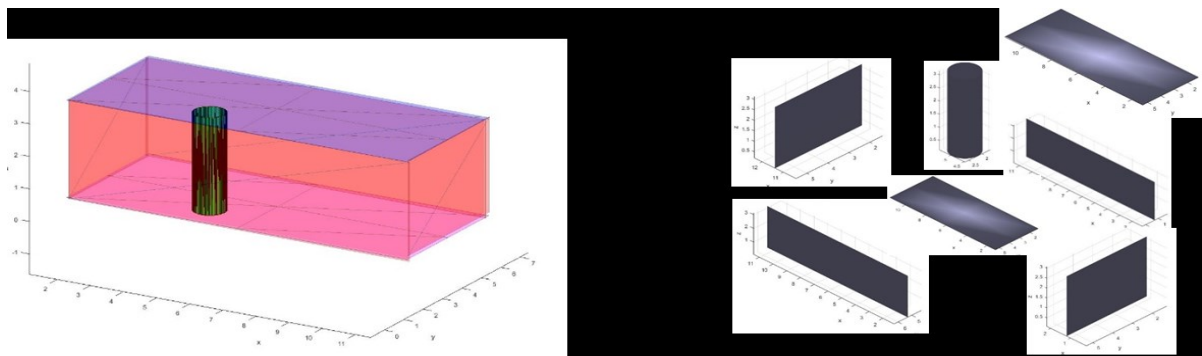
551
552

(b)

553 Figure 3- 6: (a) Horizontal plane elements region of interests and (b) Pseudocode of process flow

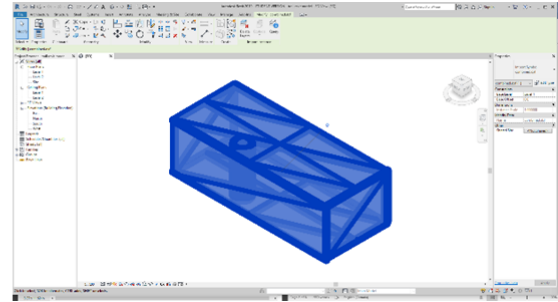
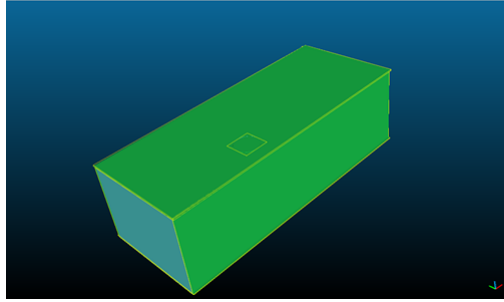
554 **3.4 Surface Reconstruction**

555 Since columns might have different diameters and heights in the buildings, an automated
556 model-fitting algorithm is needed to reconstruct the columns from the 3D-PCD. In this respect,
557 RANSAC is deployed to fit cylinder models in the segmented 3D-PCD belonging to the columns
558 from step 3.3. The cylinder models created by RANSAC can adapt the heights and diameters of
559 the columns' 3D-PCD. The cylinder models created in this step with the plane models developed
560 in previous steps are used to develop stereolithography (STL) models. The STL file format is
561 chosen as an exporting format for the 3D models, as it can be imported by many software and
562 flexible to be converted to other formats. To create an STL file for a model, a triangulated mesh
563 grid is used to represent it. Therefore, the suggested method uses the plane and cylinder models
564 created in previous steps as a base to fit a triangulated mesh grid shown in (Figure 3- 7- a). These
565 mesh grids create the STL files for each of the building elements a shown in (Figure 3- 7- b) which
566 are able to be transformed as a DWG file format using CloudCompare a shown in (Figure 3- 7- c)
567 to establish the flexibility so that reconstructed models can be imported into CAD software such
568 as Autodesk AutoCAD and Revit a shown in (Figure 3- 7- d).



569
570 (a) Mesh Surfaces Creation

(b) STL Files Creation



571

572

(c) Transforming STL Files to DWG

(d) Importing to Revit

573

Figure 3- 7: Surface reconstruction procedure

574 3.5 Evaluation Matrix

575 In terms of identification and segmentation of the building elements, the proposed
576 methodology is evaluated by the following four criteria: accuracy, recall, precision, and F1 score.

577 In addition, the capability of the proposed methodology to reconstruct suitable and accurate 3D
578 representations for the building elements is evaluated by calculating the difference and deviation
579 between the reconstructed models and the original 3D-PCD. Before explaining the identification
580 and segmentation evaluation matrix, the parameters as input in the evaluation matrix are defined:

581 (1) true positives (TP) are the number of building elements which are identified correctly; (2) false
582 negatives (FN) are the number of existing building elements which are existed but not identified;

583 (3) false positives (FP) are the number of building elements which do not exist but identified; and

584 (4) total number (TN) is total number of each type of the building elements. It should be noted that
585 the results for accuracy, recall, precision, and F1 range from 0 to 1 where 0 is a failure and 1 is a

586 total success. Accuracy is the ratio between the correctly identified building element and the total
587 number of building elements satisfying Eq. (3). Accuracy is the simplest measure of performance

588 since it provides a general overview of how the proposed method is performing. However, it does

589 not provide important information in which the proposed methodology misidentifies the building
590 elements.

591
$$Accuracy = \frac{TP}{TN} \quad (3)$$

592 Precision calculated by Eq. (4) is the ratio between the correctly identified building elements
593 and the summation of both the correctly and incorrectly identified building elements. The precision
594 indicates the capability of the proposed methodology which is to reconstruct the number of the
595 building elements without the reconstruction of the false-positive building elements.

596
$$Precision = \frac{TP}{TP+FP} \quad (4)$$

597 The recall satisfying Eq. (5) represents the ability of the proposed methodology which
598 identifies the same number of the building elements as ones existed in the building. That is, this
599 criterion is reduced when the proposed methodology does not identify the existing building
600 elements.

601
$$Recall = \frac{TP}{TP+FN} \quad (5)$$

602 F1 score calculated by Eq. (6) is to measure the overall accuracy of the proposed method based
603 on the consideration of FP and FN building elements. In other words, it is a more detail level of
604 accuracy whether or not the proposed methodology misidentifies and/or misses the building
605 elements.

606
$$F1 = 2 \times \frac{Precision \times Recall}{Precision + Recall} \quad (6)$$

607 To evaluate the capability of the proposed methodology to develop suitable and accurate 3D
608 representations for the building elements, this research uses two criteria which are size differences
609 and deviations (*i.e.*, orientation and location) between the 3D-PCD of the building elements and
610 the reconstructed 3D model. The 3D-PCD was used as the ground truth in this comparison since

611 the laser scanner utilized to capture this data is highly accurate with an error margin of millimeters.
612 Furthermore, the accuracy of the laser scanner was tested manually to ensure the measurements of
613 the dimensions are as accurate as possible to the as-built conditions. More details about the laser
614 scanner are available in the implementation section. In terms of the size differences, As shown in
615 Table 3- 1, the parameters depending on the types of the building elements are evaluated between
616 the building element’s 3D-PCD and the reconstructed 3D model. For example, the columns are
617 evaluated by the differences of the diameters and heights between 3D-PCD and the reconstructed
618 3D model. The deviation is computed to identify the differences in locations and orientations of
619 the building elements between the building elements 3D-PCD and the reconstructed mesh.
620 Accordingly, CloudCompare is utilized to determine the mean distance (MD) which is an average
621 value of the maximum and minimum distances between the building elements in 3D-PCD and the
622 reconstructed 3D mesh. Consequently, a high deviation in terms of location or/and orientation
623 between the 3D-PCD and reconstructed model leads to an increase in the MD measured by
624 CloudCompare.

625 Table 3- 1: Parameters of each building element

Building element	Size Difference				Deviation	
	Height	Diameter	Length	Width	Location	Orientation
Columns	✓	✓			✓	✓
Walls	✓		✓		✓	✓
Ceilings			✓	✓	✓	✓
Floors			✓	✓	✓	✓
Staircase (Runs)			✓	✓	✓	✓
Staircase (Rises)	✓		✓		✓	✓

626

CHAPTER 4: IMPLEMENTATION AND RESULTS

627

628 This chapter describes the application, validation and evaluation results of the proposed
629 methodology in the previous chapter. To do so, three different real-life cases were chosen to
630 validate the effectiveness of the proposed methodology. The proposed methodology
631 implementation and results will be presented in the upcoming sections.

632 4.1 Implementation

633 To achieve the targeted objectives by this research and to test the validity of the proposed
634 method, the case studies, equipment and software used, need to be defined. This section will
635 describe the chosen cases to test the proposed method, the equipment used for data collection and
636 the required software for processing the 3D-PCD.

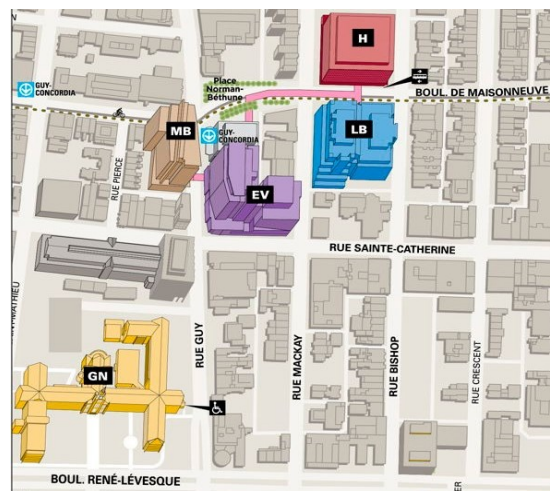
637 4.1.1 Environments

638 The proposed method is validated using three different sites at Gina Cody School of
639 engineering and computer science building, Concordia University, Sir George Williams Campus,
640 Montreal, Quebec, Canada (see Figure 4- 1). Each site is chosen to test a certain aspect of the
641 framework: (1) the lab office to test the proposed method in small simple spaces with low number
642 of features as shown in (Figure 4- 2- a); (2) the EV building entrance hall to test its ability to work
643 with multiple ceilings and columns with different dimensions and locations as shown in (Figure
644 4- 3- a); and (3) an auditorium to validate its capability to work with multiple floors and the stairs
645 illustrated in (Figure 4- 4- a). Table 4-1 summarizes the number of scans and reference targets
646 required, information about the 3D-PCD and the existing building elements, and the processing
647 time spent to run the proposed method. A different number of scans were required to generate the
648 3D-PCD for each of the 3 case studies and the reasons as follows: (1) for the lab, it is a small

649 confined space with only one column, therefore, only two scans were required at both sides of the
650 column to minimize the blind spots caused by the column preventing loss of 3D-PCD. (2) for the
651 entrance hall, it is a larger space with 6 columns, therefore, five scans were required from different
652 angles in the space to minimize the blind spots caused by the columns preventing loss of 3D-PCD.
653 (3) for the auditorium, three scans were required from different angles and elevations in the space
654 to minimize the blind spots caused by the chairs preventing loss of 3D-PCD. For visualization,
655 (Figure 4- 2- b), (Figure 4- 3- b), and (Figure 4- 4- b) show the locations of setting up the 3D Laser
656 scanner to capture the as-built condition for the spaces and acquire the 3D-PCD that the proposed
657 method will be validated and evaluated by, more details about the laser scanner will be discussed
658 in the upcoming section.

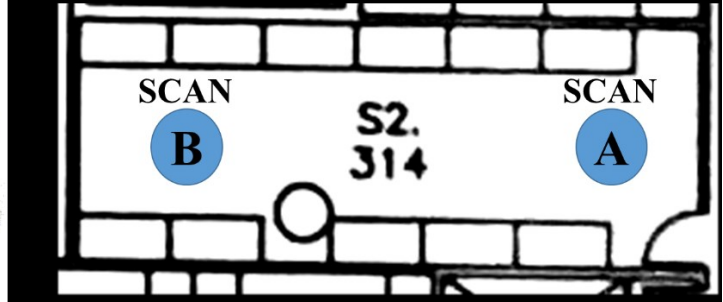


(a)



(b)

661 Figure 4- 1: (a) EV building, and (b) EV building location in SGW Campus (Concordia
662 University, 2019)



663

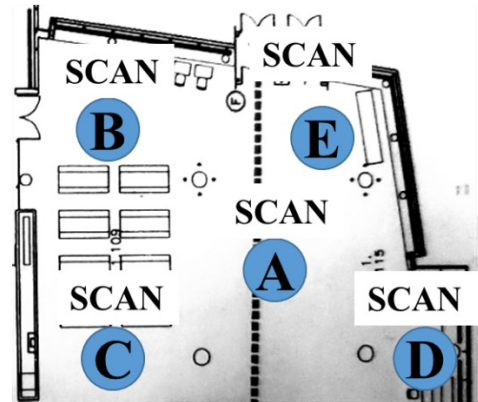
664

665

(a)

(b)

Figure 4- 2: (a) Lab office 3D-PCD, and (b) Lab office 2D plane and scan locations



666

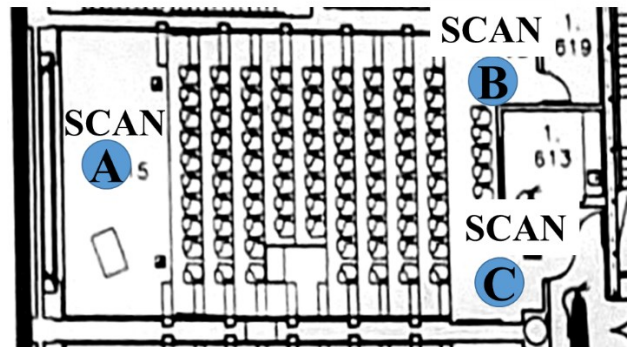
667

668

(a)

(b)

Figure 4- 3: (a) EV entrance hall 3D-PCD, and (b) EV entrance hall 2D plane and scan locations



669

670

671

(a)

(b)

Figure 4- 4: (a) Auditorium 3D-PCD, and (b) Auditorium 2D plane and scan locations

672

Table 4- 1: Case study information

Location	# of walls	# of columns	# of ceilings	# of floors	# of stairs steps	# of Points	# of Scans	# of reference spheres
Lab	4	1	1	1	0	4,658,215	2	3
EV Hall	3	6	2	1	0	4,568,841	5	5
Auditorium	6	0	1	2	9	9,364,616	3	5

673

674 4.1.2 Hardware

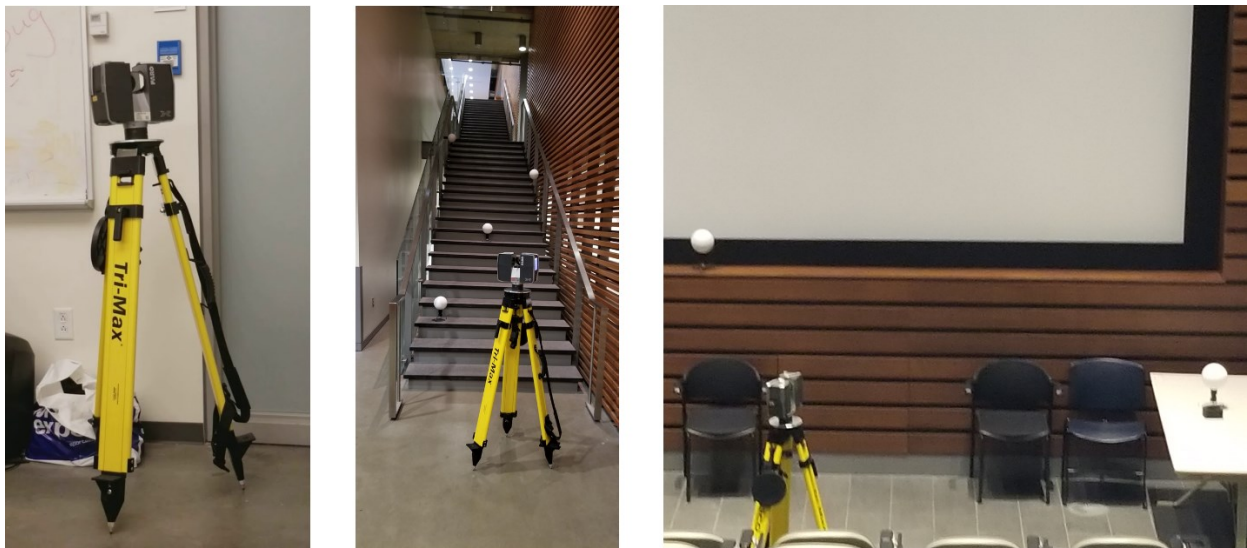
675 This section will discuss the equipment required for data collection of the as-built conditions
676 of the three test cases in the form of 3D-PCD, and for 3D-PCD processing and applying the
677 proposed methodology. These pieces of equipment are as follow:

678 1. Equipment used for 3D-PCD collection:

679 To generate the 3D-PCD for the three test cases, a laser scanner “Faro Focus 3D x 130” was
680 used. This laser scanner was chosen to collect the 3D-PCD as it was available in the lab. The
681 accuracy of the scans collected by this laser scanner was compared to other 3D-PCD collection
682 methods (i.e., stitching images). It was clear that the accuracy of the laser scanner was higher than
683 the other methods. Therefore, it was chosen as the data collection method for the proposed method
684 since it was important to accurately collect the dimensions of the building elements. The laser
685 scanner was deployed to scan the three test cases and collect 3D point clouds by scanning multiple
686 times in each case to cover the whole scanned space. To combine these multiple scans (also called
687 as registration process) reference targets were needed, therefore spherical targets were utilized in
688 the test cases to combine and align the 3D-PCDs. It is important to note that the spherical reference

689 targets should be on different planes and at least three of them are visible by the scanner in each
690 scan, this is for the alignment and combination process of the 3D-PCD (Faro Inc., 2020).

691 Technical specifications for the laser scanner that affected this research are available in Table
692 4-2 (Faro Inc., 2020; Lafi, 2017). The range of the laser scanner is 130 m which is the reason for
693 the naming, which was sufficient for the chosen case studies spaces, however, it was noticed in
694 the case of EV entrance hall, columns at larger heights had sparse 3D-PCD. The ranging error of
695 the laser scanner is ± 2 mm, which is enough to measure the dimensions of the building elements
696 existing in the 3D-PCD. The field of view (FOV) of the laser scanner covers the entire horizontal
697 angles. however, the FOV for the vertical angle is 300° the missing part is in the form of the
698 circular hole beneath the laser scanner, therefore, to fill these holes, multiple scans in the spaces.



699

700 Figure 4- 5: Laser scanner and spherical reference targets deployment

701

702

703

704

705 Table 4- 2: Technical specifications for the laser scanner (Faro Inc., 2020; Lafi, 2017)

Laser Scanner	Faro Focus 3D x 130
Range	0.6 - 130 m
Measurement speed	122,000 - 976,000 pts/sec
Ranging error	±2 mm
Field of view (vertical/horizontal)	300° / 360°

706

707 2. Equipment used for 3D-PCD processing:

708 To process the 3D-PCD gathered by the laser scanner, and to apply the proposed method to
 709 reconstruct it, Razer Blade 15 laptop was used. This laptop was used to register the multiple scans
 710 gathered by the laser scanner, clean the 3D-PCD from outliers, and finally develop, apply and
 711 evaluate the proposed method. Technical specifications for the laptop used in this research are
 712 available in Table 4- 3.

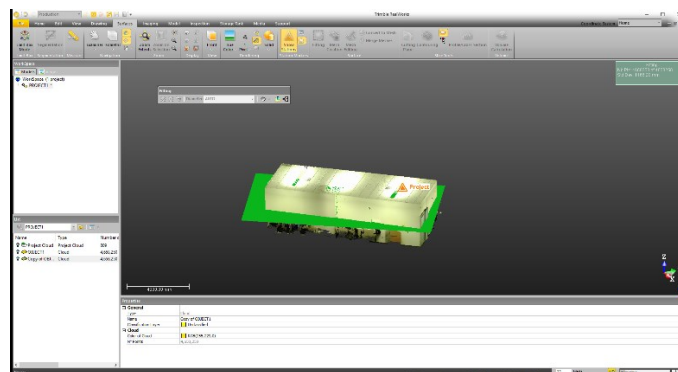
713 Table 4- 3: Technical specifications for the Laptop (Faro Inc., 2020; Lafi, 2017)

Laptop	Razer Blade 15
Processor	Intel Core i7 CPU @ 2.20 GHz
RAM memory	16.0 GB (2 x 8.0 GB) DDR4
Storage space	512 GB (SSD)
Graphics Card	NVIDIA GeForce GTX 1070 Max-Q Design
Operating system	Windows 10 Home 64-bit operating system

714

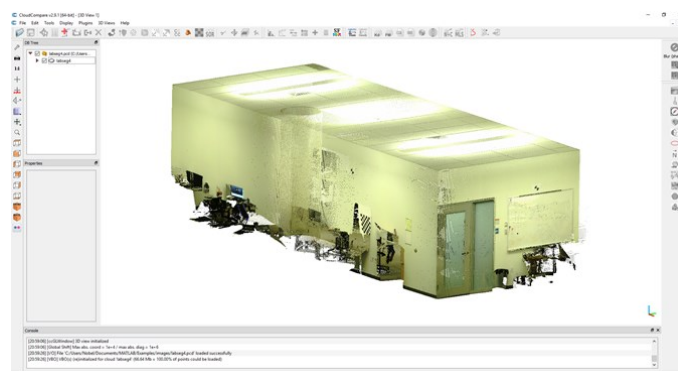
715 4.1.3 Software

716 To align and combine (register) all the scans gathered by the laser scanner and create the 3D-
717 PCD, Trimble Real works 10.0.4 was used since it was the software associated with the laser
718 scanner (Trimble, 2019). CloudCompare 2.10.2 was used for a multiple of reasons throughout the
719 research: (1) Downsizing and cleaning the 3D-PCD as mentioned in the methodology chapter; (2)
720 measuring the dimensions of the building elements in the 3D-PCD for evaluation; and (3)
721 calculating the mean distances between the reconstructed model and the 3D-PCD (Compare,
722 2019). The methods introduced in this research are developed and applied using MATLAB
723 R2017a, using some toolboxes and functions available in the Math Works library (The Math Works,
724 2019). Finally, Blender 2.81 was used to give thickness and colors to each of the building elements
725 for better visualization as shown in Figure 4- 8 (Blender Org., 2020).



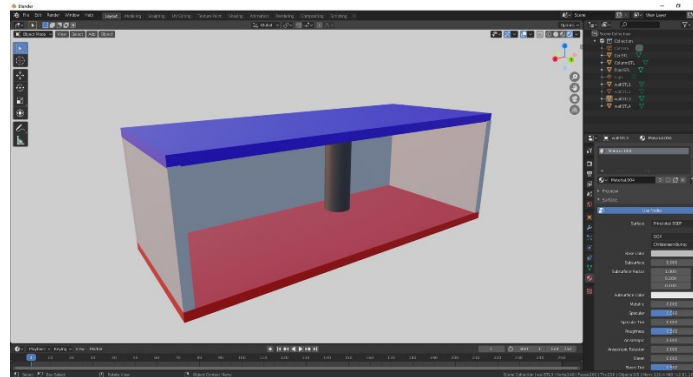
726

727 Figure 4- 6: Registering the 3D-PCD using Trimble Real Works software



728

729 Figure 4- 7: Cleaning the 3D-PCD from outliers using CloudCompare software



730
731 Figure 4- 8: Applying colors to the final 3D reconstructed model using Blender software

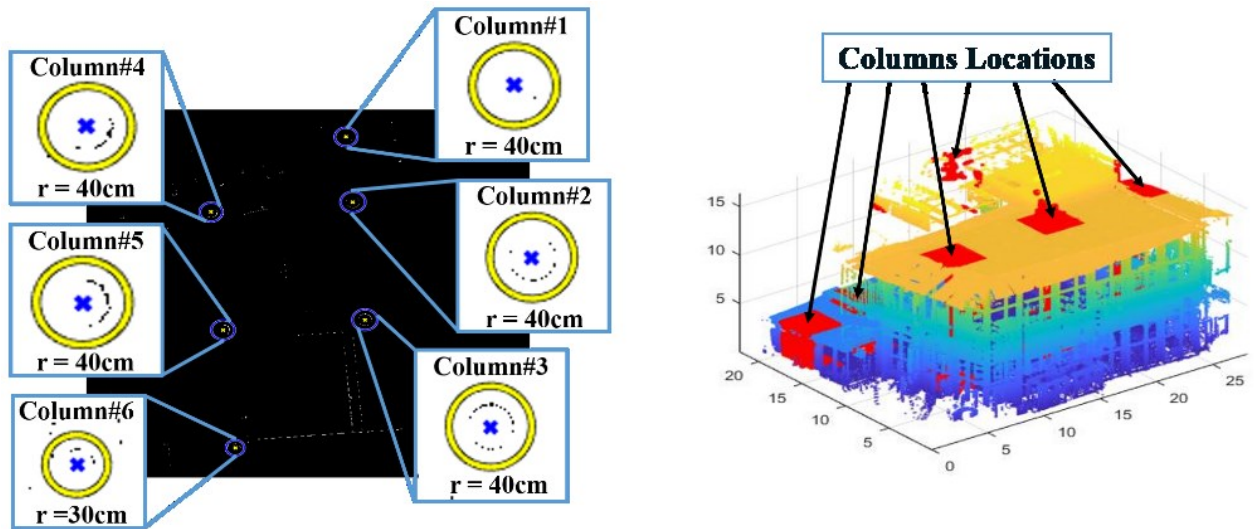
732 4.2 Results

733 This section will discuss the application, results, and evaluation of the proposed method on
734 the three test cases. It should be noted that this research does not represent the procedures for the
735 transformation of the 3D-PCD to 2D image and 3D reconstruction since this research follows the
736 common procedures in 3D reconstruction studies.

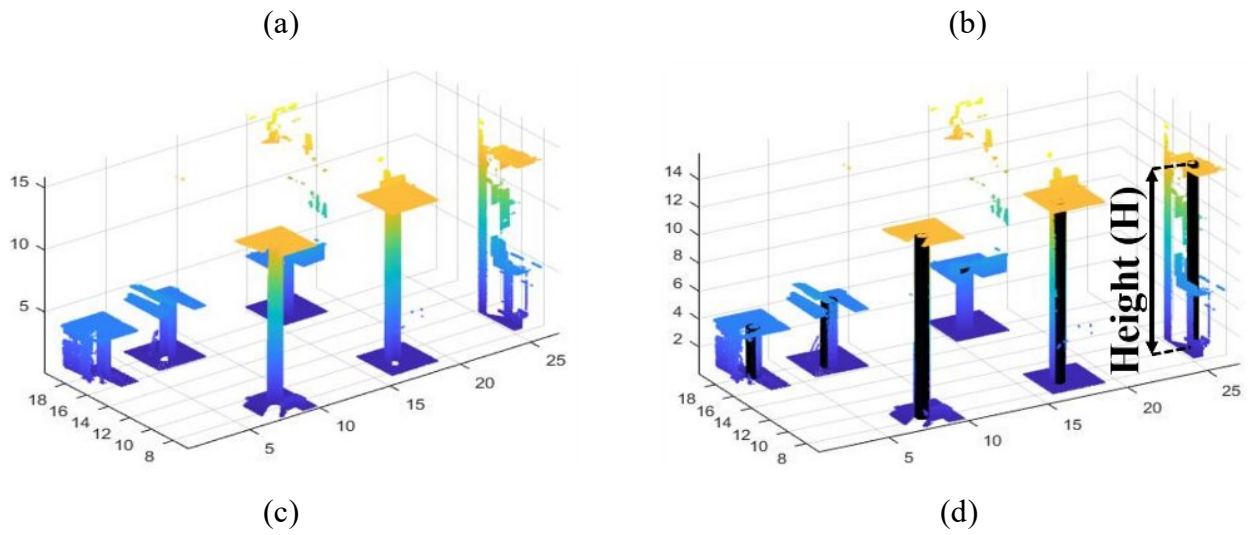
737 4.2.1 Vertical plane building elements

738 EV building entrance hall is used to test the capability of the proposed method to identify,
739 segment, and reconstruct columns involving different dimensions. Based on the 2D image, as
740 shown in (Figure 4- 9- a), Hough circle transform (HCT) captures the column information such as
741 the number of columns which are six columns, their locations and center points, and radii. This
742 information is used to define the region of interests (ROIs) located on the center points of the
743 columns in order to not only prevent the loss of 3D-PCD but also facilitate the segmentation of the
744 columns. In this respect, since the ROIs are represented as rectangular boxes, the dimensions of
745 the ROIs (the lengths and widths) are $78\text{ cm} \times 78\text{ cm}$ and $104\text{ cm} \times 104\text{ cm}$ when the radii of the
746 columns are 30 cm and 40cm, respectively. These ROIs are projected into the 3D-PCD to identify

747 and select the columns-related 3D-PCD as shown in (Figure 4- 9- b) and to segment them
 748 illustrated in (Figure 4- 9- c). Instead of the number of iterations defined by users manually for the
 749 segmentation, this study uses six times determined by the number of columns resulted from the
 750 HCT. In this respect, as illustrated in (Figure 4- 9- d) RANSAC is deployed six times to fit cylinder
 751 surface models in the segmented 3D-PCD of columns adapting to the dimensions of the columns.



752
753



754
755
756

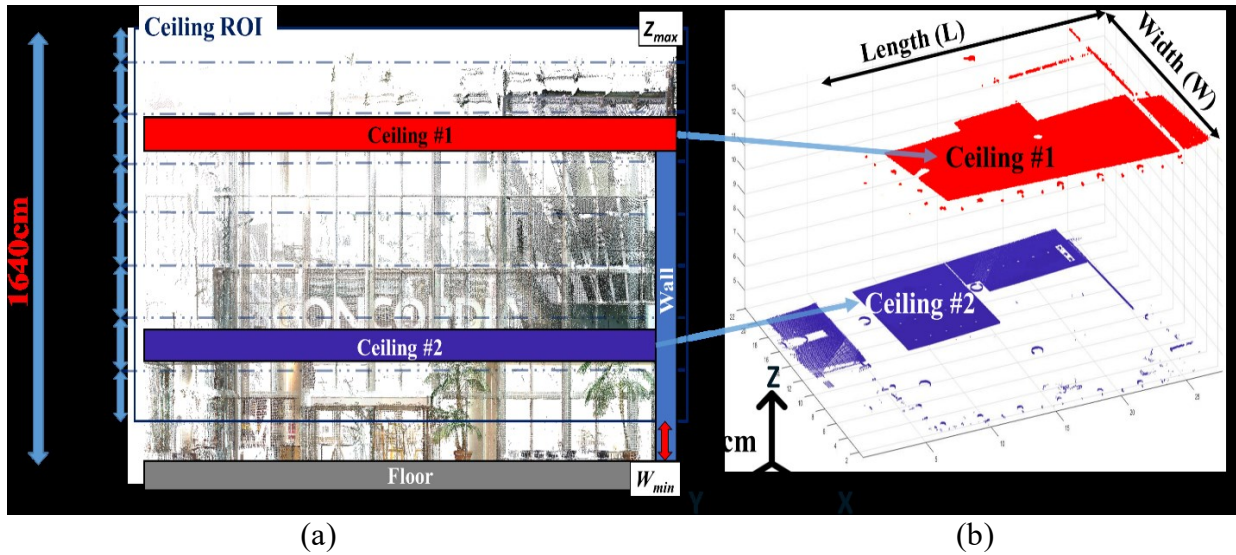
Figure 4- 9: Identification and segmentation of columns

757 As one of the vertical plane building elements, the walls in the auditorium are identified,
758 segmented, and reconstructed. Since the walls are represented as lines in the 2D image, Hough line
759 transform (HLT) is implemented to identify the wall information including the number of walls
760 where are six, locations, and the lengths which are from 160 cm to 1480 cm. To develop the
761 automated segmentation of the walls using the vertical plane RANSAC, the number of iterations
762 is defined as six which are the same as the number of walls identified by the HLT. As a result,
763 plane RANSAC segments and build wall plane models that involve the same dimensions and
764 locations as ones in real. However, walls #5 and #6 were segmented together, and the last iteration
765 of RANSAC segmented the screen in the auditorium.

766 4.2.2 Horizontal plane building elements

767 EV building entrance hall is used to validate the capability of the proposed method to identify,
768 segment, and reconstruct multiple ceilings, while the auditorium case was utilized for multiple
769 floors and stairs. As discussed earlier, the horizontal plane building elements are identified and
770 segmented by a heuristic approach that implements vertical and/or horizontal plane RANSAC
771 iteratively on the ROIs of the 3D-PCD in accordance with the types of the building elements. In
772 this respect, the ceiling ROI is defined from 200 cm above the lowest Z coordinate among the
773 walls, which is $W_{min} = 0$ cm, to $Z_{max} = 1640$ cm which is the highest Z coordinate among the 3D-
774 PCD. As a result, the height of the ceiling ROI is 1440 cm which is relatively a large area including
775 two ceilings. As represented in (Figure 4- 10- a), the ROI of the ceilings is subdivided by 200 cm.
776 In this respect, there are a total of seven sub-ROIs that have the same height but the last one is 40
777 cm. In addition, the number of the sub-ROIs is used to determine the number of iterations to run
778 the horizontal plane RANSAC (eight iterations) in order to not only identify and segment multiple
779 ceilings but also constructing preliminary surface models utilized for the reconstruction process.

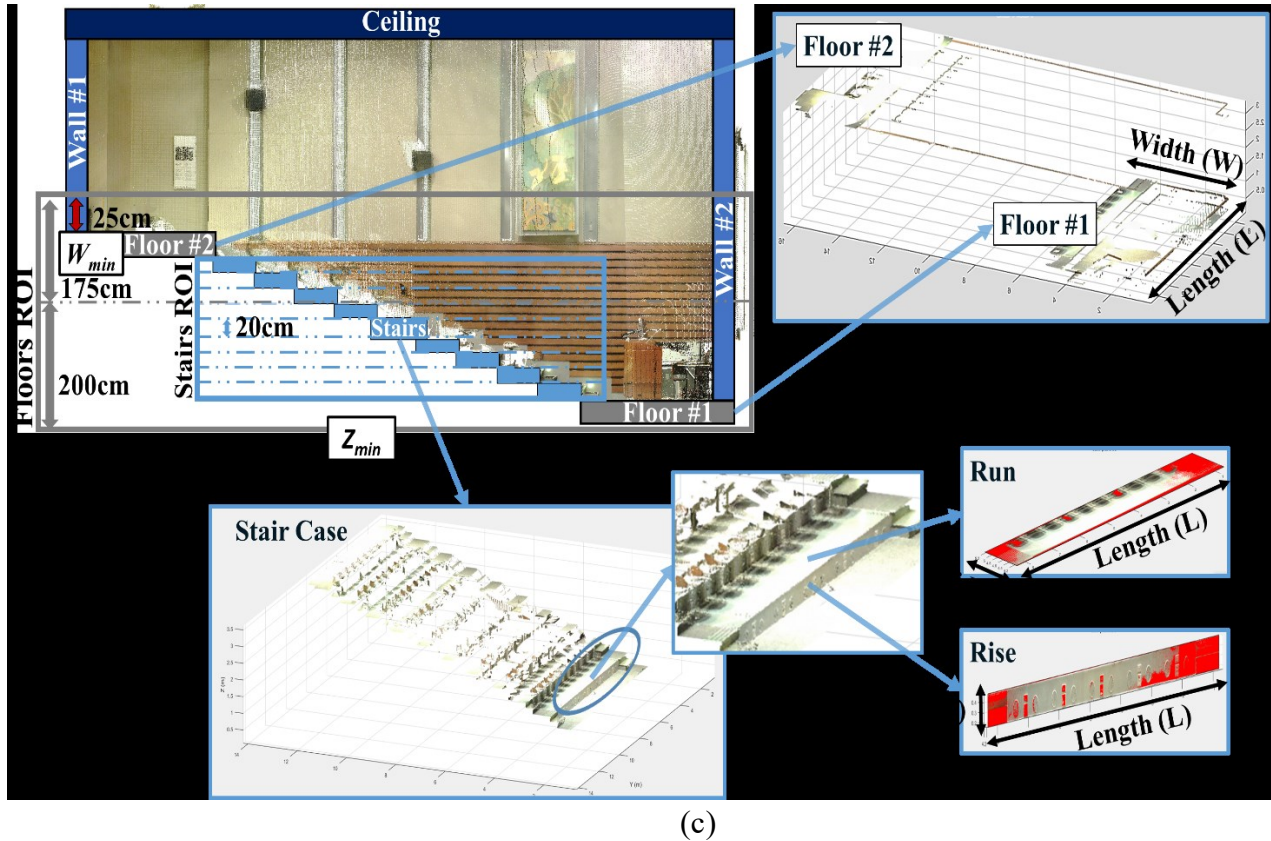
780 (Figure 4- 10- b) represents a result of ceiling identification, segmentation and surface
781 development.



784 Figure 4- 10: Identification and segmentation of ceilings

785 The identification and segmentation of the floors are implemented based on similar procedures
786 to ones used in the ceiling identification and segmentation. However, the auditorium case involves
787 six walls which are used to determine whether or not there are multiple floors and staircase based
788 on the comparison of the wall heights. Since there are different wall heights, 800 cm, and 450 cm,
789 the auditorium space has two floors and one staircase. In this respect, the floor ROI is defined from
790 0 cm which is the lowest Z coordinate of the 3D-PCD to 375 cm which is calculated by adding 25
791 cm from the lowest Z coordinate among six walls ($W_{min} = 350$ cm). As shown in (Figure 4- 11- a),
792 this ROI is subdivided into two sub-ROIs which have 200 cm and 175 cm heights. The horizontal
793 plane RANSAC has been run twice in accordance with the number of the sub-ROIs to identify and
794 segment the floors represented in (Figure 4- 11- b). To allow people access to these floors, the
795 stairs consisting of the nine runs and rises, illustrated in (Figure 4- 11- c), are identified and

796 segmented by the vertical and horizontal plane RANSAC running eighteen times each which are
797 a number of the staircase sub-ROIs divided the staircase ROI (0 cm to 350 cm) by 20 cm.



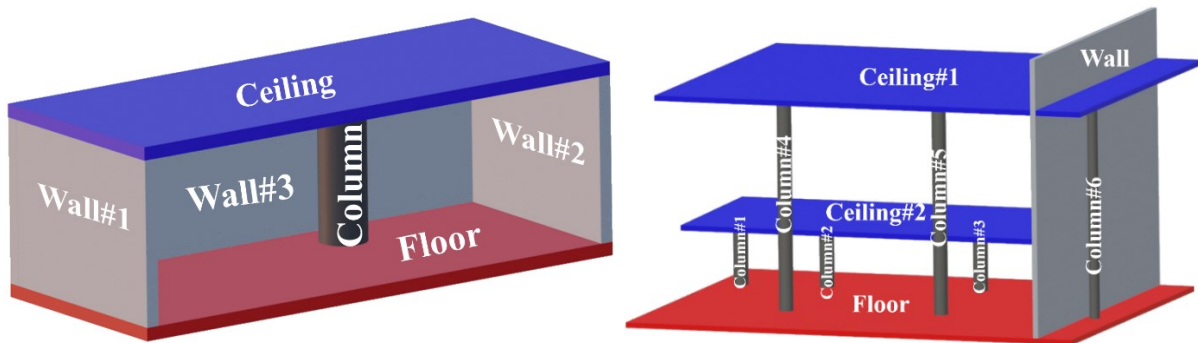
799 Figure 4- 11: Floors and stairs identification and segmentation

800 4.2.3 Evaluation

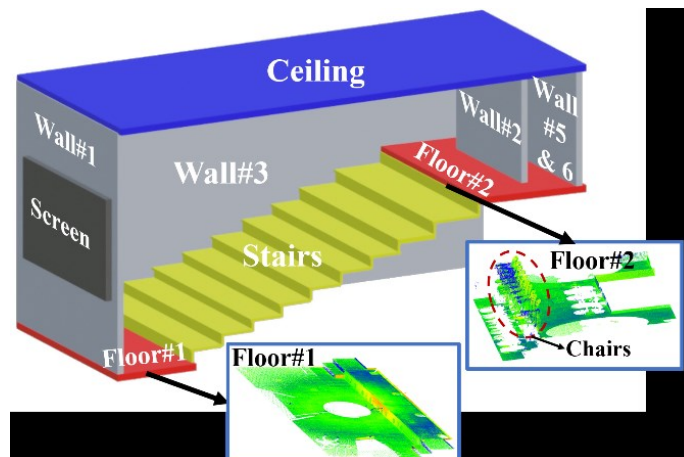
801 Although the proposed method identifies, segments and reconstructs the building elements
802 successfully, the reconstructed models are shown in Figure 4- 12 should be evaluated by the
803 proposed matrix to validate the effectiveness of the proposed method. In terms of the total
804 computation time, the proposed method takes approximately 125, 130, and 500 seconds to
805 reconstruct 3D models for lab office, EV entrance hall and auditorium cases respectively. The
806 increase in the processing time for the case of the auditorium is due to the existence of stairs which
807 requires to run vertical and horizontal plane RANSAC eighteen times, respectively. To evaluate

808 the performance of the proposed identification and segmentation, four criteria, which are accuracy,
 809 recall, precision, and F1 score, are measured based on one column, ceiling, floor and four walls in
 810 the lab office, six columns and two ceilings in the EV entrance hall and two floors, six walls and
 811 a staircase with 9 stairs in the auditorium. As shown in Table 4- 4, columns, ceilings, stairs, and
 812 floors have the highest scores among the four criteria in which the proposed method is
 813 implemented efficiently and effectively without identification and segmentation of false positive
 814 and negative building elements. However, the walls in the auditorium have 0.83 in precision since
 815 plane RANSAC recognizes wall #5 and #6 as one wall and the screen (vertical planar shape) as
 816 the other wall even though the Hough line transform identifies six walls accurately. Due to the
 817 reconstruction of the false-positive wall, the F1 score is reduced as 0.91. However, the recall and
 818 accuracy are not affected by the precision and F1 score since all the walls are identified, segmented
 819 and reconstructed.

820



821



822 Figure 4- 12: Reconstruction results of Lab office, EV entrance hall, and auditorium (sidewall #4
 823 is removed for visualization in both the lab and auditorium case studies)

824 Table 4- 4: Results of the evaluation matrix

Test Case	Building Element	Accuracy	Precision	Recall	F1 score
Lab Office	Column	1	1	1	1
	Floor	1	1	1	1
	Ceiling	1	1	1	1
	Walls	1	1	1	1
EV Entrance	Column	1	1	1	1
Hall	Ceiling	1	1	1	1
Auditorium	Stairs	1	1	1	1
	Floor	1	1	1	1
	Walls	1	0.83	1	0.91

825

826 Although the performance of the proposed methodology is evaluated by the criteria described
 827 above, there is not sure whether or not the 3D reconstructed models are built corresponding to the
 828 building elements in 3D-PCD in terms of dimensions, locations, and orientations. In this respect,
 829 the size differences and deviation are measured based on the result of the 3D reconstruction process
 830 and the 3D-PCD. The different types of size differences are used in accordance with the types of
 831 building elements. As a result, the size differences and deviation are represented in Table 4- 5. The
 832 positive values indicate that the building elements in 3D-PCD are larger than the reconstructed 3D
 833 model while the negative values are vise versa. The minimum size differences are represented in

834 the diameters of the columns and heights and lengths of the walls. In this respect, the size
835 difference ranges between 1 cm and 10 cm which are relatively lower than 90 cm in other studies
836 (Franz et al., 2018; Murali et al., 2017; Valero, Adán, & Bosché, 2016). Even though the size
837 difference exhibited by the proposed method is an improvement compared to previous approaches,
838 to the best knowledge of the author, there is no standardized threshold or a technique that can be
839 used to know whether this size difference is acceptable or not. Other size differences of the
840 building elements are measured largely with high variances even though the type of the building
841 elements is the same and located in the same building space. For example, the height differences
842 of the columns are varied from 4 cm to 45 cm in the case of the EV entrance hall due to the large
843 scale of the building space and occlusion during the scanning. However, in the lab office which is
844 smaller and more confined space compared to the EV entrance hall, the column exhibited a low
845 size difference of less than 1 cm. Moreover, although the floor #1 is reconstructed successfully
846 with low size differences, 5 cm in length and 13 cm in width, the floor #2 has high size differences,
847 93 cm in length and 36 cm in width, due to the chairs shown in Figure 4- 11 leading to consider as
848 a part of the floor by the planar RANSAC. Within this reason, the size differences of the runs and
849 rises in the staircase range from 0 cm to 45 cm. In terms of the deviation, the proposed
850 methodology reconstructs the 3D building elements with a relatively low deviation ranging from
851 0.6 cm to 9 cm. Based on the consideration of the multi-level building spaces, the proposed
852 methodology has a lower location (LOC) and orientation (ORI) deviation in the ceilings, floors,
853 and runs and rises in the staircase than ones in the columns and walls.

854

Table 4- 5: Results of the size difference and deviation

Test Case	Building element	Size Difference				Deviation	
		H (cm)	D (cm)	L (cm)	W (cm)	LOC (cm)	ORI (cm)
Lab office	Ceiling	-	-	-3	-2	0.8	-
	Floor	-	-	-6	-6	-	0.6
	Column	-0.3	-0.5	-	-	2.8	-
	Wall #1	-1	-	-5	-	-	2.1
	Wall #2	4	-	-9	-	3.2	-
	Wall #3	3	-	-5	-	1.8	-
	Wall #4	-3	-	1	-	0.9	-
EV	Column #1	15	3	-	-	7.7	-
Entrance	Column #2	4	1	-	-	7.0	-
Hall	Column #3	35	-1	-	-	6.0	-
	Column #4	45	2	-	-	3.0	-
	Column #5	30	1	-	-	6.0	-
	Column #6	34	-1	-	-	9.0	-
	Ceiling #1	-	-	-27	-7	3.0	-
	Ceiling #2	-	-	18	38	1.8	-
Auditorium	Wall #1	-4	-	3	-	-	2.8
	Wall #2	3	-	-8	-	0.5	-
	Wall #3	2	-	-4	-	-	2.4
	Wall #4	6	-	-6	-	0.6	-
	Wall #5 & #6	7	-	-10	-	2.8	-
	Floor #1	-	-	5	13	0.3	-
	Floor #2	-	-	-93	36	0.4	-
	Staircase (Rise)	4 (0)*	-	45 (1)*	-	-	5.0 (1.0)*
	Staircase (Run)	-	-	30 (2)*	10 (1)*	0.6 (0.3)*	-

*The values of the staircase indicate the maximum and minimum

CHAPTER 5: CONCLUSION AND FUTURE WORKS

858

859 5.1 Summary

860 Accurate 3D representation for as-built conditions of buildings is essential in the renovation
861 and remodeling industry to develop as-built 3D models used to generate the shop drawings with
862 time and cost-saving. In this respect, the reconstruction procedures generally consist of: (1)
863 identification and segmentation of building elements; and (3) reconstructing the segmented
864 building elements 3D-PCD. However, these procedures, especially identification and
865 segmentation, tend to be tedious, manual, error-prone and time-consuming tasks due to the
866 perception-based number of iterations, over- or under-segmentation of the building elements from
867 3D-PCD, and uncertainty to reconstruct the 3D building elements in multi-level building space. In
868 this respect, this research proposes an automatic 3D geometric reconstruction approach which
869 mainly focuses on developing the efficient and effective identification and segmentation process
870 using Hough circle and line transform techniques, region of interest, and plane RANSAC. The
871 proposed 3D-PCD reconstruction system consists of the following steps: (1) cleaning and
872 preparing the 3D-PCD; (2) transforming 3D-PCD to a 2D image; (3) identification and
873 segmentation of building elements; and (4) reconstructing the segmented building elements 3D-
874 PCD into simple forms such as planes and cylinders. The proposed method offers the following
875 benefits: (1) the fully automated process with very little input by the user, able to identify, segment
876 and reconstruct building elements such as columns, stairs, walls, ceilings, and floors.; (2)
877 efficiency improvement by defining the number of iterations for RANSAC, instead of being
878 arbitrarily given by the user while retaining high accuracy in terms of identification and
879 segmentation; (3) error reduction and accuracy improvement of the reconstruction process by

880 defining the locations and small areas where RANSAC will be implemented, reducing the effect
881 of outliers on it; and (4) expanding upon the applicability of the reconstruction process by taking
882 into consideration multi-level space such as cinemas and auditoriums with multi-ceiling and/or
883 floors, stairs and columns. The end-user for the proposed method is expected to be the modeling
884 architect who is tasked to construct a 3D model that represent the as-built conditions and later on
885 use it for remodeling or apply changes to the scanned environment. The effectiveness of the
886 proposed framework is evaluated in accuracy, precision, recall, and F1 score. The proposed
887 method was able to identify and segment almost all targeted building elements in the three cases
888 studies used to test the proposed method. In the detail level of the evaluation, the ceilings, floors,
889 and stairs in multi-level building spaces are reconstructed successfully with low location and
890 orientation deviation.

891 **5.2 Future Works**

892 In the future, the proposed methodology could be improved by: (1) reconstruct window walls
893 such as glass facades in the building; (2) improve the size difference and deviation between the
894 3D-PCD and the reconstructed model are required to improve caused by furniture existing in the
895 scanned space; (3) investigate different 3D scanners and/or methods to improve the quality of the
896 scanned 3D-PCD; (4) taking into consideration slanted ceilings, walls, columns, and floors would
897 improve the applicability of the proposed method; (5) expanding on the identified elements by
898 adding openings such as windows and doors for better representation of the as-built conditions of
899 the scanned environment; (6) creating connections between building elements and creating the IFC
900 models for the development of the building information modeling (BIM); (7) identifying the
901 materials of the building elements based on the RGB information of the 3D-PCD ; (8) exploring
902 the benefits of combining multiple data acquisition methods such as stitching digital images and

903 laser scanner; and (9) exploring the possibility of adding structural information such as steel rebars
904 existing in the concrete building elements.

905

REFERENCES

- 906
- 907 3DReshaper. (2019). 3DReshaper. Retrieved 20 October, 2019, from
- 908 <https://www.3dreshaper.com/fr/>
- 909 Anagnostopoulos, I., Pătrăucean, V., Brilakis, I., & Vela, P. (2016). *Detection of walls, floors,*
- 910 *and ceilings in point cloud data.* Paper presented at the Construction Research Congress
- 911 2016.
- 912 association, C. H. b. (2019). Economic Impacts of the Housing Industry. Retrieved 2 August,
- 913 2019, from
- 914 https://www.chba.ca/CHBA/Housing_in_Canada/Information_and_Statistics/Information
- 915 [Statistics.aspx](https://www.chba.ca/CHBA/Housing_in_Canada/Information_and_Statistics/Information)
- 916 Azhar, S., Khalfan, M., & Maqsood, T. (2012). Building information modeling (BIM): now and
- 917 beyond. *Construction Economics and Building*, 12(4), 15-28.
- 918 Berger, M., Tagliasacchi, A., Seversky, L. M., Alliez, P., Guennebaud, G., Levine, J. A., . . .
- 919 Silva, C. T. (2017). *A survey of surface reconstruction from point clouds.* Paper presented
- 920 at the Computer Graphics Forum.
- 921 Chen, J., Cho, Y. K., & Kim, K. (2018). *Region proposal mechanism for building element*
- 922 *recognition for advanced scan-to-BIM process.* Paper presented at the Construction
- 923 Research Congress 2018.
- 924 Chen, J., Kira, Z., & Cho, Y. K. (2019). Deep learning approach to point cloud scene
- 925 understanding for automated scan to 3D reconstruction. *Journal of Computing in Civil*
- 926 *Engineering*, 33(4), 04019027.
- 927 Chida, A., & Masuda, H. (2016). Reconstruction of polygonal prisms from point-clouds of
- 928 engineering facilities. *Journal of Computational Design and Engineering*, 3(4), 322-329.

929 Choi, S., Kim, T., & Yu, W. (1997). Performance evaluation of RANSAC family. *Journal of*
930 *Computer Vision*, 24(3), 271-300.

931 Compare, C. (2019). CloudCompare 3D point cloud and mesh processing software Open Source
932 Project. Retrieved 20 October, 2019, from <https://www.danielgm.net/cc/>

933 Delage, E., Lee, H., & Ng, A. Y. (2007). Automatic single-image 3d reconstructions of indoor
934 manhattan world scenes *Robotics Research* (pp. 305-321): Springer.

935 Díaz-Vilariño, L., Conde, B., Lagüela, S., & Lorenzo, H. (2015). Automatic detection and
936 segmentation of columns in as-built buildings from point clouds. *Remote Sensing*, 7(11),
937 15651-15667.

938 Dimitrov, A., & Golparvar-Fard, M. (2015). Segmentation of building point cloud models
939 including detailed architectural/structural features and MEP systems. *Automation in*
940 *Construction*, 51, 32-45.

941 Ding, L., & Goshtasby, A. (2001). On the Canny edge detector. *Pattern Recognition*, 34(3), 721-
942 725.

943 Eric Levenson, M. B. a. E. G. (2019). A fire gutted parts of Notre Dame Cathedral and altered
944 the Paris skyline. Retrieved 18 February 2020, from
945 <https://www.cnn.com/2019/04/15/world/notre-dame-cathedral-fire/index.html>

946 Franz, S., Irmeler, R., & Rüppel, U. (2018). Real-time collaborative reconstruction of digital
947 building models with mobile devices. *Advanced Engineering Informatics*, 38, 569-580.

948 Furukawa, Y., Curless, B., Seitz, S. M., & Szeliski, R. (2009). *Manhattan-world stereo*. Paper
949 presented at the 2009 IEEE Conference on Computer Vision and Pattern Recognition.

950 Giakoumelis, G., & Lam, D. (2004). Axial capacity of circular concrete-filled tube columns.
951 *Journal of Constructional Steel Research*, 60(7), 1049-1068.

952 Gilbert, B. (2019). As France rebuilds Notre-Dame Cathedral, the French studio behind
953 'Assassin's Creed' is offering up its 'over 5,000 hours' of research on the 800-year-old
954 monument. Retrieved 18 February 2020, from [https://www.businessinsider.com/notre-](https://www.businessinsider.com/notre-dame-fire-assassins-creed-maxime-durand-ubisoft-interview-2019-4)
955 [dame-fire-assassins-creed-maxime-durand-ubisoft-interview-2019-4](https://www.businessinsider.com/notre-dame-fire-assassins-creed-maxime-durand-ubisoft-interview-2019-4)

956 Grilli, E., Menna, F., & Remondino, F. (2017). A review of point clouds segmentation and
957 classification algorithms. *The International Archives of Photogrammetry, Remote Sensing*
958 *and Spatial Information Sciences*, 42, 339.

959 Hong, S., Jung, J., Kim, S., Cho, H., Lee, J., & Heo, J. (2015). Semi-automated approach to
960 indoor mapping for 3D as-built building information modeling. *Computers, Environment*
961 *and Urban Systems*, 51, 34-46.

962 Huber, D., Akinici, B., Oliver, A. A., Anil, E., Okorn, B. E., & Xiong, X. (2011). *Methods for*
963 *automatically modeling and representing as-built building information models*. Paper
964 presented at the Proceedings of the NSF CMMI Research Innovation Conference.

965 Inc., F. T. (2020). Faro Focus 3D x 130. Retrieved 22 February, 2020, from
966 <https://www.faro.com/>

967 Jung, J., Hong, S., Jeong, S., Kim, S., Cho, H., Hong, S., & Heo, J. (2014). Productive modeling
968 for development of as-built BIM of existing indoor structures. *Automation in*
969 *Construction*, 42, 68-77.

970 Lafi, G. A. (2017). *3D thermal modeling of built environments using visual and infrared sensing*.
971 (Masters of applied sciences), Concordia University.

972 Li, M., Wonka, P., & Nan, L. (2016). *Manhattan-world urban reconstruction from point clouds*.
973 Paper presented at the European Conference on Computer Vision.

974 Li, S., Isele, J., & Bretthauer, G. (2008). Proposed methodology for generation of building
975 information model with laserscanning. *Tsinghua Science and Technology*, 13(S1), 138-
976 144.

977 Lu, R., Brilakis, I., & Middleton, C. R. (2019). Detection of structural components in point
978 clouds of existing RC bridges. *Computer-Aided Civil and Infrastructure Engineering*,
979 34(3), 191-212.

980 Lu, X., Yao, J., Tu, J., Li, K., Li, L., & Liu, Y. (2016). PAIRWISE LINKAGE FOR POINT
981 CLOUD SEGMENTATION. *ISPRS Annals of Photogrammetry, Remote Sensing &*
982 *Spatial Information Sciences*, 3(3).

983 Lyons, K. (2019). Notre Dame fire: Macron promises to rebuild cathedral within five years.
984 Retrieved 18 February, 2020, from
985 [https://www.theguardian.com/world/2019/apr/17/notre-dame-fire-macron-promises-to-](https://www.theguardian.com/world/2019/apr/17/notre-dame-fire-macron-promises-to-make-cathedral-more-beautiful-than-before)
986 [make-cathedral-more-beautiful-than-before](https://www.theguardian.com/world/2019/apr/17/notre-dame-fire-macron-promises-to-make-cathedral-more-beautiful-than-before)

987 Macher, H., Landes, T., & Grussenmeyer, P. (2015). Point clouds segmentation as base for as-
988 built BIM creation. *ISPRS Annals of the Photogrammetry, Remote Sensing and Spatial*
989 *Information Sciences*, 2(5), 191.

990 Macher, H., Landes, T., & Grussenmeyer, P. (2017). From point clouds to building information
991 models: 3D semi-automatic reconstruction of indoors of existing buildings. *Applied*
992 *Sciences*, 7(10), 1030.

993 Murali, S., Speciale, P., Oswald, M. R., & Pollefeys, M. (2017). *Indoor scan2bim: Building*
994 *information models of house interiors*. Paper presented at the 2017 IEEE/RSJ
995 International Conference on Intelligent Robots and Systems (IROS).

996 Ochmann, S., Vock, R., & Klein, R. (2019). Automatic reconstruction of fully volumetric 3D
997 building models from oriented point clouds. *ISPRS journal of photogrammetry and*
998 *remote sensing*, 151, 251-262.

999 Oesau, S., Lafarge, F., & Alliez, P. (2014). Indoor scene reconstruction using feature sensitive
1000 primitive extraction and graph-cut. *ISPRS Journal of Photogrammetry and Remote*
1001 *Sensing*, 90, 68-82.

1002 ONTARIO, Q. S. P. F. (2017). THE ONTARIO BUILDING CODE ONLINE. Retrieved 14
1003 January, 2020, from <http://www.buildingcode.online/>

1004 Org., B. (2020). Open source 3D creation. Free to use for any purpose, forever. Retrieved 22
1005 February 2020, from <https://www.blender.org/>

1006 Pătrăucean, V., Armeni, I., Nahangi, M., Yeung, J., Brilakis, I., & Haas, C. (2015). State of
1007 research in automatic as-built modelling. *Advanced Engineering Informatics*, 29(2), 162-
1008 171.

1009 Pérez-Sinticala, C., Janvier, R., Brunetaud, X., Treuillet, S., Aguilar, R., & Castañeda, B. (2019).
1010 Evaluation of Primitive Extraction Methods from Point Clouds of Cultural Heritage
1011 Buildings *Structural Analysis of Historical Constructions* (pp. 2332-2341): Springer.

1012 Qi, C. R., Su, H., Mo, K., & Guibas, L. J. (2017). *Pointnet: Deep learning on point sets for 3d*
1013 *classification and segmentation*. Paper presented at the Proceedings of the IEEE
1014 Conference on Computer Vision and Pattern Recognition.

1015 Rwamamara, R., Norberg, H., Olofsson, T., & Lagerqvist, O. (2010). Using visualization
1016 technologies for design and planning of a healthy construction workplace. *Construction*
1017 *Innovation*, 10(3), 248-266.

1018 Schnabel, R., Wahl, R., & Klein, R. (2007). *Efficient RANSAC for point-cloud shape detection*.
1019 Paper presented at the Computer graphics forum.

1020 Tallon, A. (2014). Divining Proportions in the Information Age. *Architectural Histories*, 2(1).

1021 Tarsha-Kurdi, F., Landes, T., & Grussenmeyer, P. (2007). *Hough-transform and extended ransac*
1022 *algorithms for automatic detection of 3d building roof planes from lidar data*. Paper
1023 presented at the ISPRS Workshop on Laser Scanning 2007 and SilviLaser 2007.

1024 Tatarchenko, M., Dosovitskiy, A., & Brox, T. (2017). *Octree generating networks: Efficient*
1025 *convolutional architectures for high-resolution 3d outputs*. Paper presented at the
1026 Proceedings of the IEEE International Conference on Computer Vision.

1027 MathWorks. (2019). MATLAB. Retrieved 31 December, 2019, from
1028 <https://www.mathworks.com/products/matlab.html>

1029 Thomson, C., & Boehm, J. (2015). Automatic geometry generation from point clouds for BIM.
1030 *Remote Sensing*, 7(9), 11753-11775.

1031 Trimble. (2019). Trimble RealWorks. Retrieved 31 December, 2019, from
1032 <https://geospatial.trimble.com/products-and-solutions/trimble-realworks>

1033 Ubisoft. (2019). Supporting Notre-Dame de Paris. Retrieved 18 February 2020, from
1034 [https://news.ubisoft.com/en-us/article/2Hh4JLkJ1GJIMEg0lk3Lfy/supporting-](https://news.ubisoft.com/en-us/article/2Hh4JLkJ1GJIMEg0lk3Lfy/supporting-notredame-de-paris)
1035 [notredame-de-paris](https://news.ubisoft.com/en-us/article/2Hh4JLkJ1GJIMEg0lk3Lfy/supporting-notredame-de-paris)

1036 University, C. (2019). Venue. Retrieved 21 February, 2020, from
1037 <https://www.concordia.ca/events/conferences/plundered-cultures/venue.html>

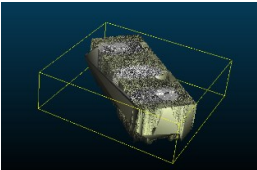
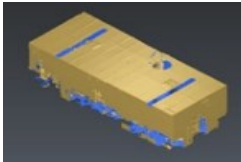
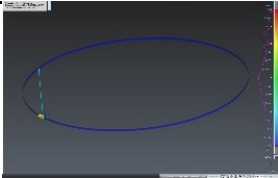
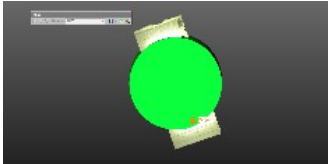
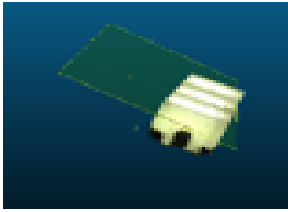
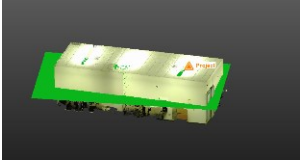

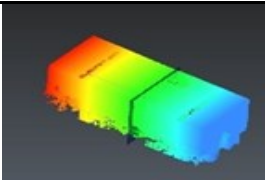
1038 Valero, E., Adán, A., & Bosché, F. (2016). Semantic 3D reconstruction of furnished interiors
1039 using laser scanning and RFID technology. *Journal of Computing in Civil Engineering*,
1040 30(4), 04015053.

- 1041 Wang, Q., Tan, Y., & Mei, Z. (2019). Computational Methods of Acquisition and Processing of
1042 3D Point Cloud Data for Construction Applications. *Archives of Computational Methods*
1043 *in Engineering*, 1-21.
- 1044 Zhang, Z., Huang, Y., Zhang, W., & Luo, J. (2017). *Comparisons of planar detection for service*
1045 *robot with RANSAC and region growing algorithm*. Paper presented at the 2017 36th
1046 Chinese Control Conference (CCC).
- 1047

1048 **APPENDIX**

1049 **1. Reconstruction results utilizing available software:**

1050 Table 6- 1: Software results in the reconstruction process

	CloudCompare	3DReshaper	Trimble Real Works
Mesh			<u>NA*</u>
Cylinder fitting	<u>NA*</u>		
Horizontal plane fitting		<u>NA*</u>	
Vertical plane fitting			<u>NA*</u>

*Not an option available in the software

1051

1052

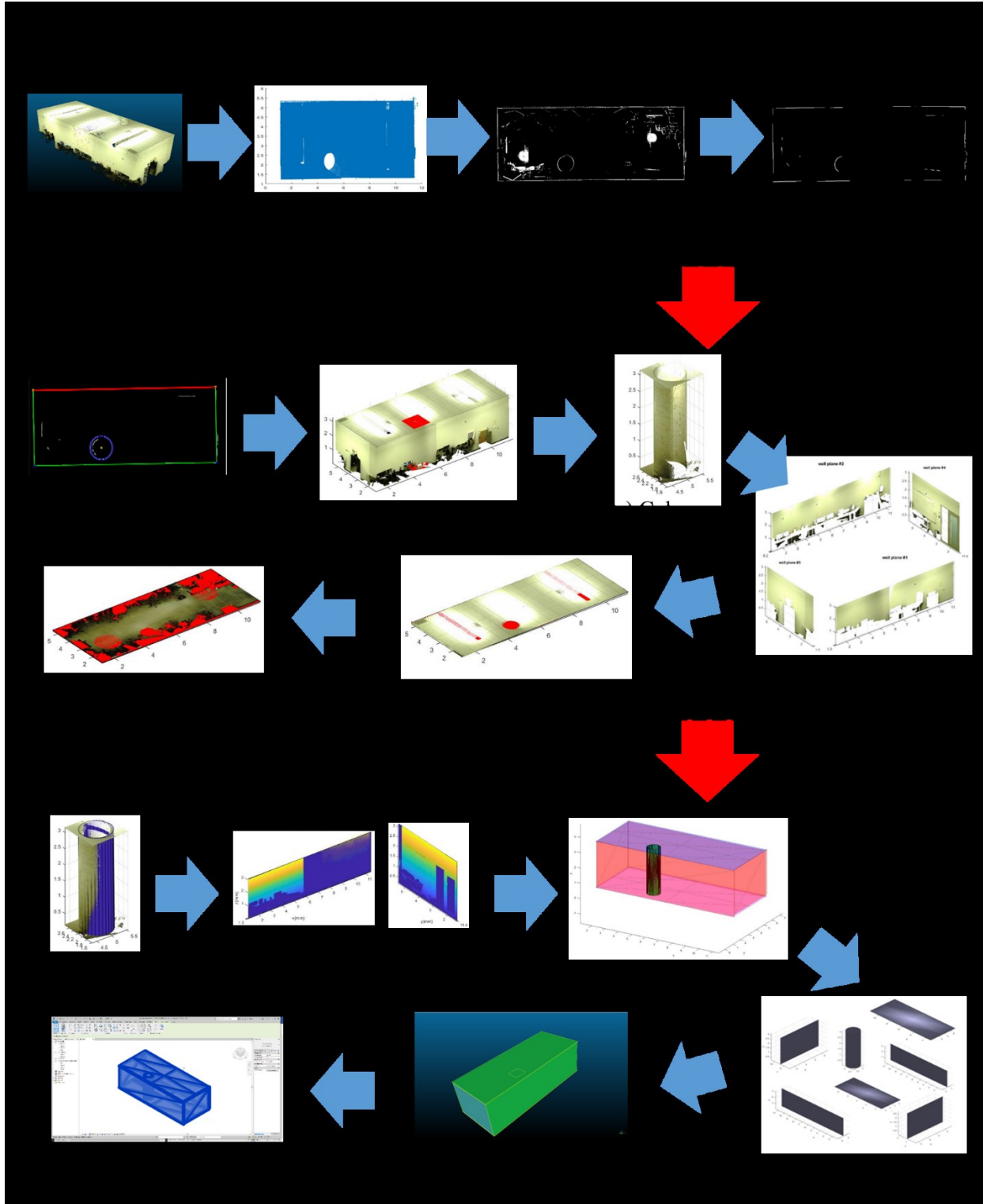
1053

1054

1055

1056

2. Results and Flowcharts of the applied methodology:



1059 Figure 6- 1: Results of each step in the Proposed methodology for the lab office case study

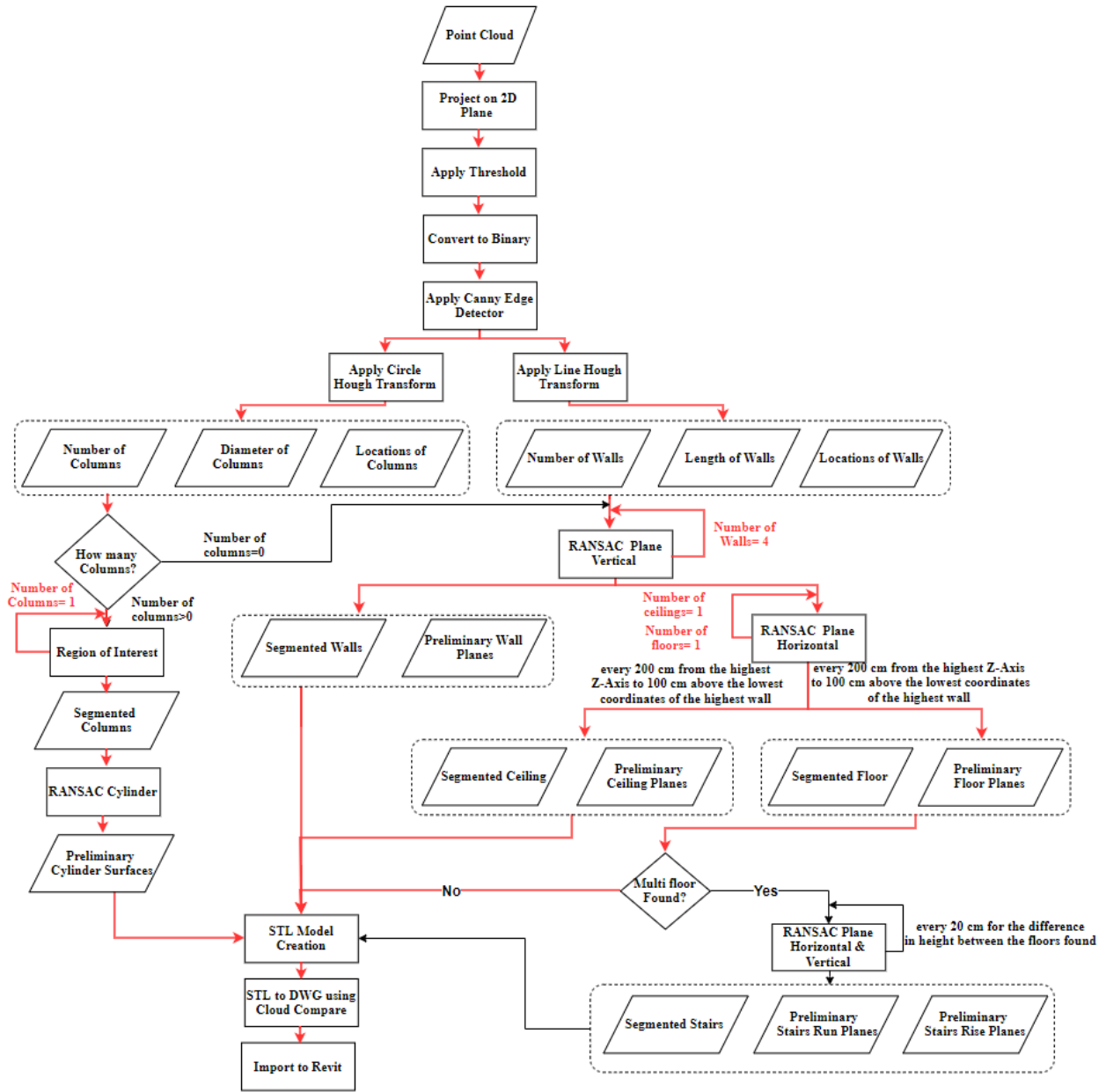
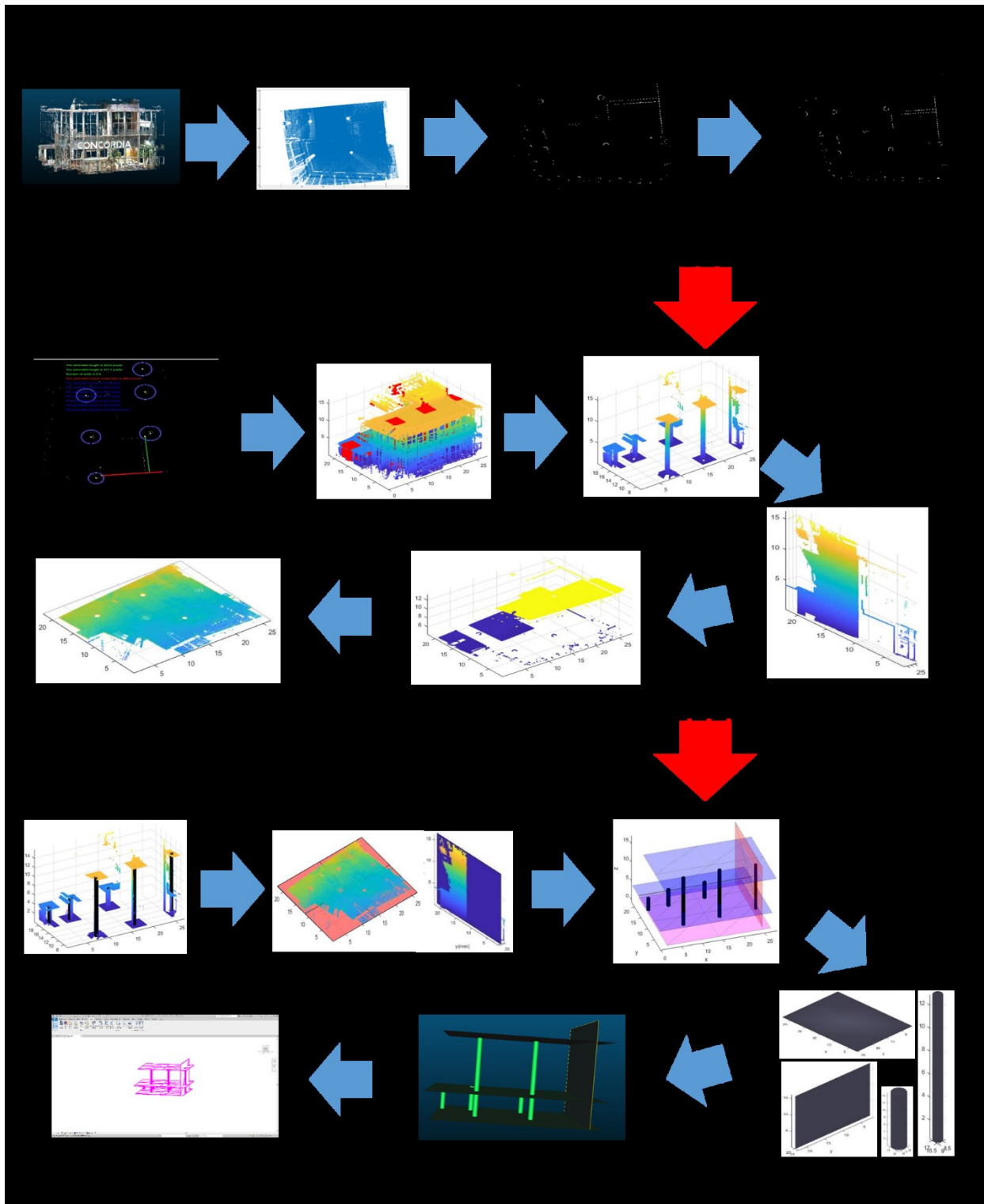


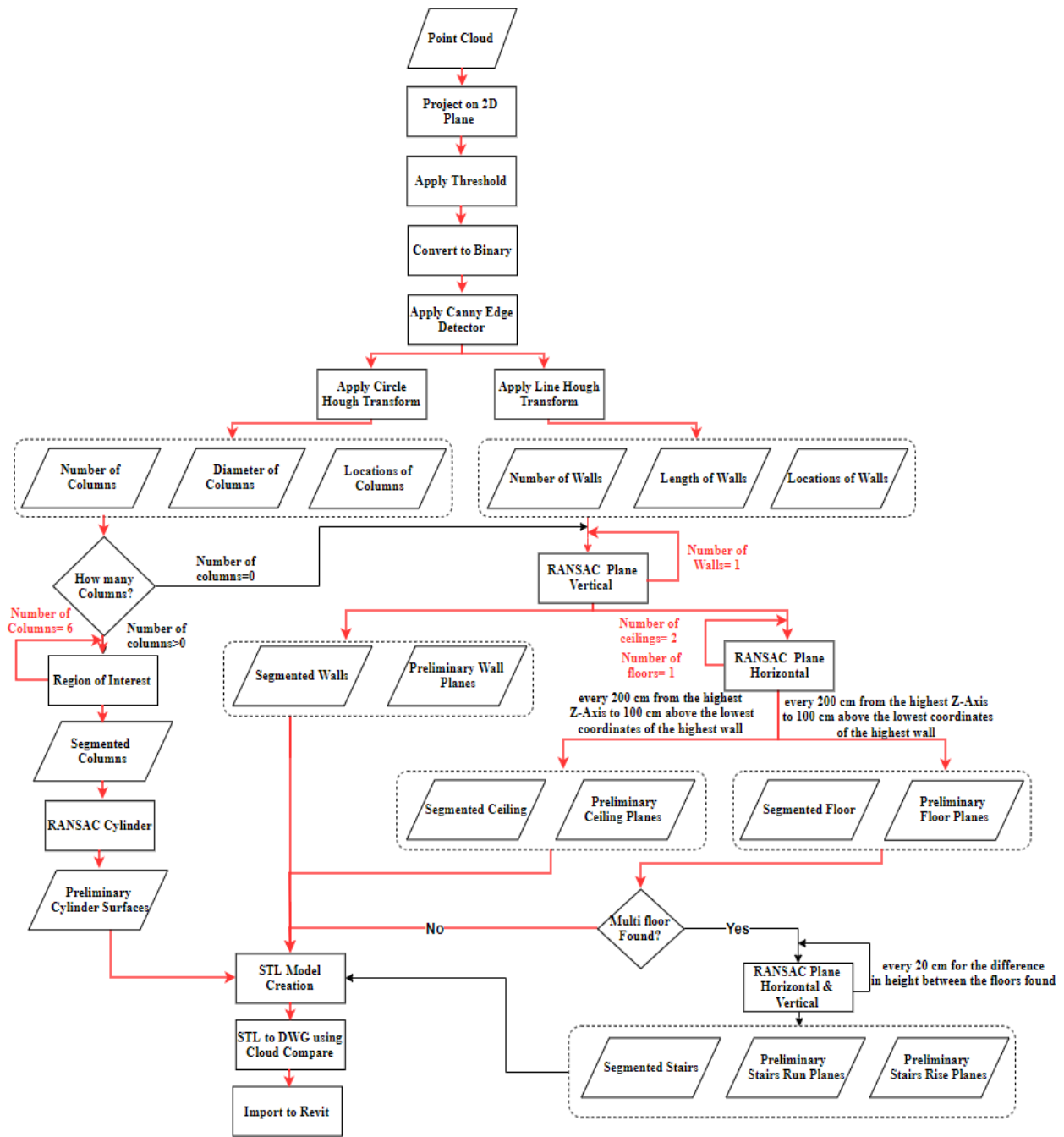
Figure 6- 2: Flowchart for the case of lab office case study



1064

1065 Figure 6- 3: Results of each step in the Proposed methodology for the EV entrance hall case
 1066 study

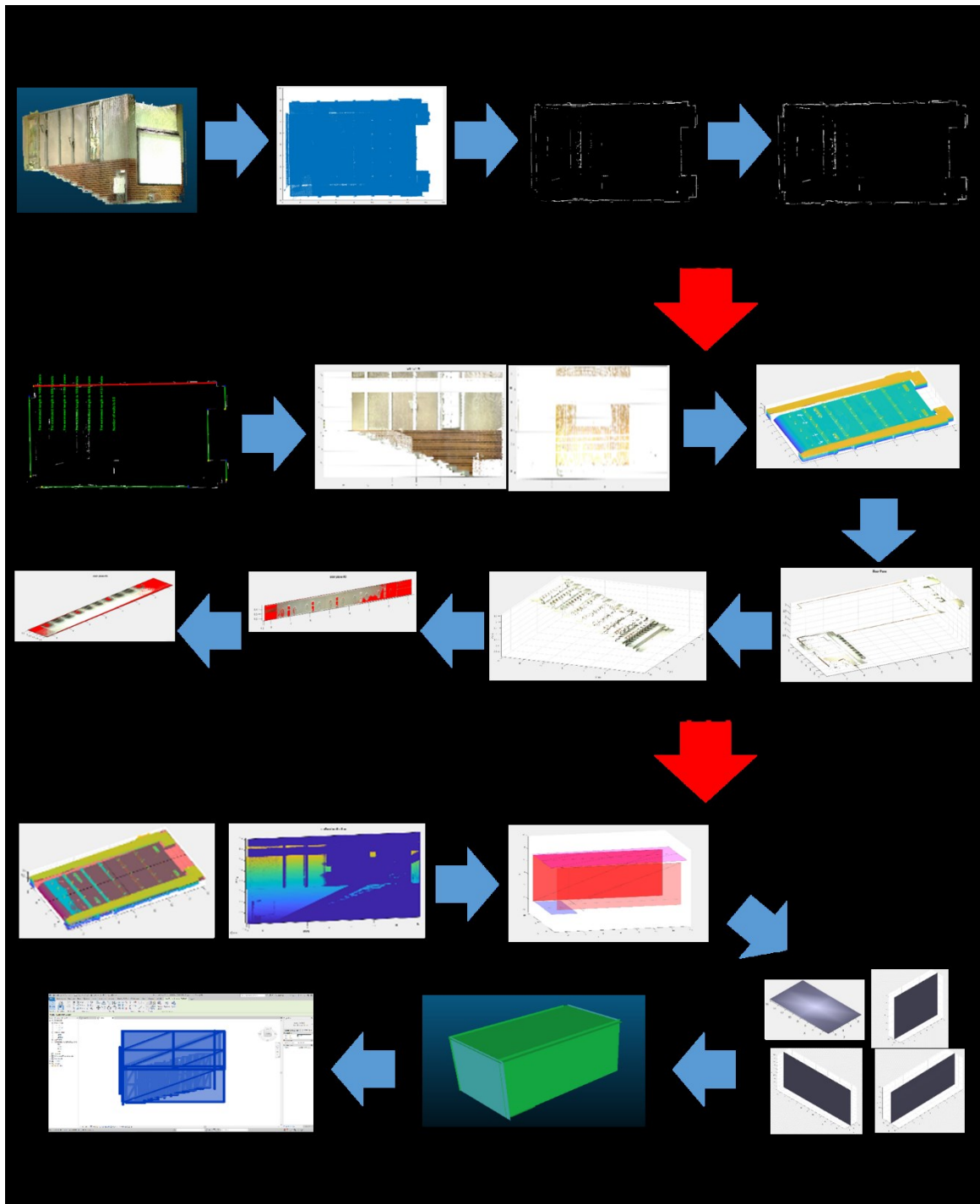
1067



1068

1069

Figure 6- 4: Flowchart for the case of EV entrance hall case study

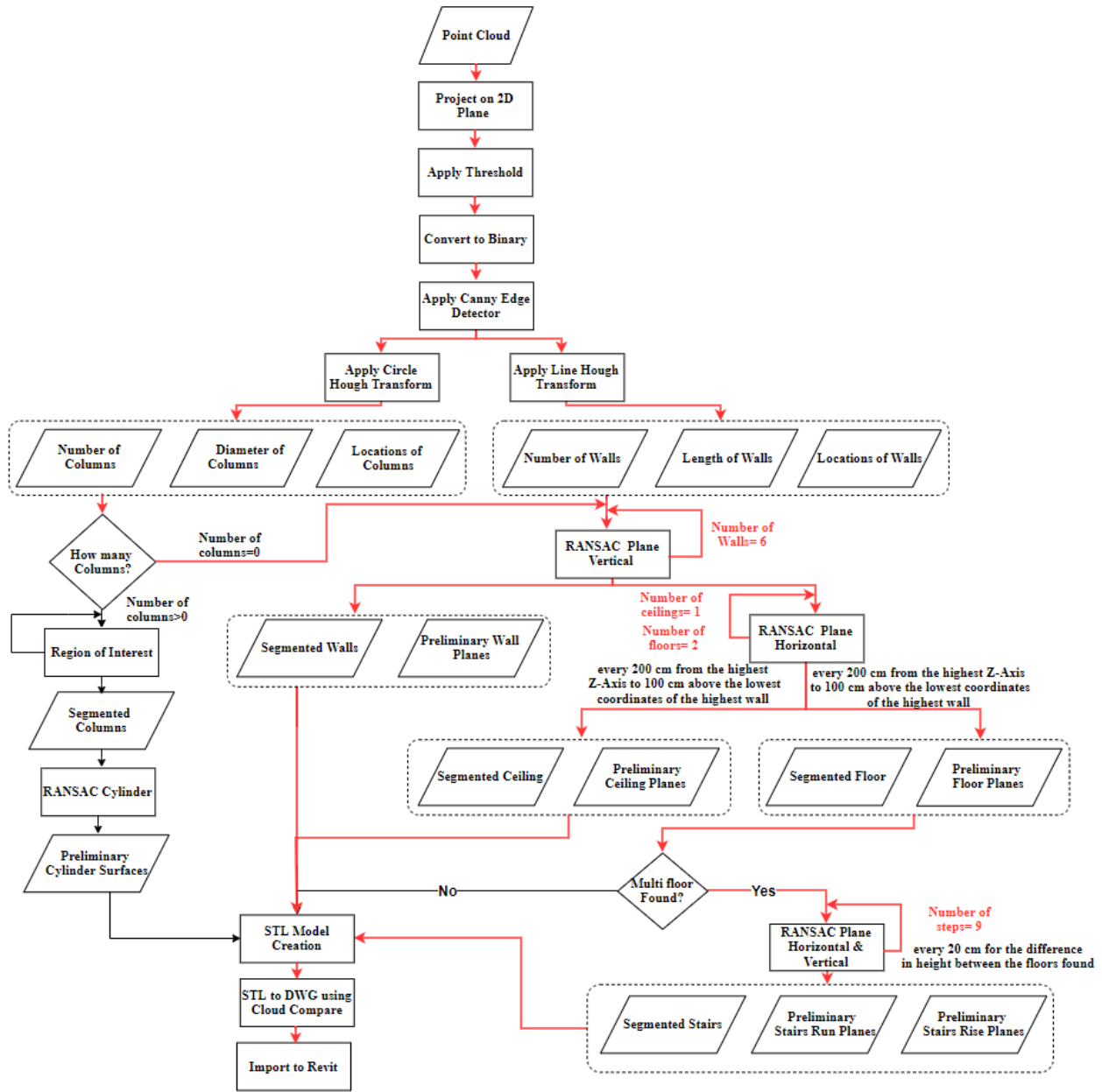


1070

1071 Figure 6- 5: Results of each step in the Proposed methodology for auditorium case study

1072

1073



1074

1075

1076

1077

1078

1079

1080

1081

Figure 6- 6: Flowchart for the case of auditorium case study

1082

3. Building elements characteristics and methods of I&S:

1083

Table 6- 2: Building elements characteristics

Type	Columns	Walls	Stairs		Ceilings	Floors
			Rise	Run		
Dimensions Considered	10 (min) D	120 (min) L/W	20 (max) H	35.5 (NI*) L/W	120*120 (NI) L&W	120*120 (NI) L&W
ROI/Location	Based on CHT	Based on LHT	Between Floors		(W_{min} +100cm) to Z_{max}	Z_{min} to (W_{min} +100cm)
Shape	Circular	Plane				
Parameters	Diameter & Height	Length & Height		Length & Width		
Orientation	Vertical			Horizontal		
Method of I&S	Hough Transform + RANSAC		RANSAC (Heuristic Approach)			

1084

*Not important for the proposed method

1085

4. Building Code of Ontario:

1086

Table 6- 3: Building Code of Ontario (ONTARIO, 2017)

Room	Area	Walls	Height
Main Bedroom	9.8 m ² (with Closets) 8.8 m ² (without)	2.7 m	2.1 m
Secondary Bedroom	7.0 m ² (with Closets) 6.0 m ² (without)	2.0 m	2.1 m
Dining room	3.25 m ²	2.3 m	2.1 m
Living room	13.5 m ²	3.0 m	2.1 m
Bathroom	-	1.2 m	2.1m
Kitchen	4.2 m ²	-	2.1 m
Doors	-	0.76 m (width)	1.98m

1087